The kinematics of the Dasht-e Bayaz earthquake fault during Pliocene-Quaternary: implications for the geodynamics of eastern Central Iran

Fariborz Baniadam, Esmaeil Shabanian, Olivier Bellier

Elsevier Editorial System(tm) for Tectonophysics

Manuscript Draft

Manuscript Number: TECTO13372R2

Title: The kinematics of the Dasht-e Bayaz earthquake fault during Pliocene-Quaternary: implications for the geodynamics of eastern Central Iran

Article Type: Research Paper

Keywords: fault kinematic analysis; paleostress; active tectonics; Dasht-e Bayaz Fault; Lut Block; Central Iran

Corresponding Author: Dr. Esmaeil Shabanian,

Corresponding Author's Institution: IASBS

First Author: Fariborz Baniadam, Ph.D. student

Order of Authors: Fariborz Baniadam, Ph.D. student; Esmaeil Shabanian; Olivier Bellier

Abstract: The Arabia - Eurasia convergence is accommodated across the Iranian plateau and surrounding mountain ranges. Strike-slip faults play significant roles in the current deformation of the Iranian plateau and were responsible for several moderate to large earthquakes, especially in east of Iran. The sinistral Dasht-e Bayaz fault shows conspicuous seismic and geological activities, while the role of the fault in the accommodation of active convergence is still debated. This paper focuses on the Pliocene-Quaternary to present-day states of stress in the region affected by the Dasht-e Bayaz fault. We applied the fault-slip inversion technique to both kinds of seismologic and geological fault slip data. The inversion results indicate a mean N045±5°E trending σ1 in the modern stress field, which agrees with the present-day tectonic regime (regional N050±05°E trending σ1) deduced from the inversion of earthquake focal mechanism data. The paleostress state is characterized by a N135±15°E trending regional mean σ1, with a transpressional stress regime; E-W faults of the region such as the Dasht-e Bayaz fault were reverse dextral in this paleostress field. We show that the shift in fault kinematics during the Pliocene-Quaternary times has not been restricted to northeastern parts of the Iranian plateau. The cross-cutting relationship between active N-S dextral and E-W sinistral faults indicates a crosswise to conjugate fault arrangement in the middle and the eastern end of the Dasht-e Bayaz fault. Integrating our results at a larger regional scale, we present a kinematic model in which the region between Lut and Kopeh Dagh is divided by the Doruneh fault into two tectonic domains. In the northern domain, active convergence is taken up by the extrusion of fault-bounded crustal blocks while, in the southern domain the convergence is accommodated through crosswise strike-slip faulting accompanied by reverse/thrust faulting in confining wedges.

Research Data Related to this Submission

The kinematics of the Dasht-e Bayaz earthquake fault during Pliocene-Quaternary: implications for the geodynamics of eastern Central Iran

Fariborz Baniadam[a b], Esmaeil Shabanian[c], Olivier Bellier[a]

[a] Aix Marseille Univ, CNRS, IRD, INRA, Coll France, CEREGE, Aix-en-Provence, France, bellier@cerege.fr

[b] Geological Survey of Iran, Tehran, Iran, baniadam@cerege.fr; fzbaniadam@gmail.com

[c] Department of Earth Sciences, Institute for Advanced Studies in Basic Sciences (IASBS), Zanjan 45137-66731, Iran, corresponding author: E-mail address: es.shabanian@gmail.com; shabanian@iasbs.ac.ir

Keywords: Fault kinematic analysis; Paleostress; Active tectonics; Dasht-e Bayaz Fault; Lut Block; Central Iran

Abstract

The Arabia - Eurasia convergence is accommodated across the Iranian plateau and surrounding mountain ranges. Strike-slip faults play significant roles in the current deformation of the Iranian plateau and were responsible for several moderate to large earthquakes, especially in east of Iran. The sinistral Dasht-e Bayaz fault shows conspicuous seismic and geological activities, while the role of the fault in the accommodation of active convergence is still debated. This paper focuses on the Pliocene-Quaternary to present-day states of stress in the region affected by the Dasht-e Bayaz fault. We applied the fault-slip inversion technique to both kinds of seismologic and geological fault slip data. The inversion results indicate a mean N045±5°E trending σ_1 in the modern stress field, which agrees with the present-day tectonic regime (regional N050±05°E trending σ_1) deduced from the inversion of earthquake focal mechanism data. The paleostress state is characterized by a N135±15°E trending regional mean σ_1, with a transpressional stress regime; E-W faults of the region such as the Dasht-e Bayaz fault were reverse dextral in this paleostress field. We show that the shift in fault kinematics during the Pliocene-Quaternary times has not been restricted to northeastern parts of the Iranian plateau. The cross-cutting relationship

between active N-S dextral and E-W sinistral faults indicates a crosswise to conjugate fault arrangement in the middle and the eastern end of the Dasht-e Bayaz fault. Integrating our results at a larger regional scale, we present a kinematic model in which the region between Lut and Kopeh Dagh is divided by the Doruneh fault into two tectonic domains. In the northern domain, active convergence is taken up by the extrusion of fault-bounded crustal blocks while, in the southern domain the convergence is accommodated through crosswise strike-slip faulting accompanied by reverse/thrust faulting in confining wedges.

1. Introduction

The convergence between Arabia and Eurasia is responsible for current deformation in Iran. Nearly all convergence is accommodated across the Iranian plateau and surrounding mountain ranges such as Zagros, Alborz and Kopeh Dagh; the collision boundaries correspond approximately to the political borders of Iran. The Makran tectonic province is the surface expression of the active subduction of Arabia beneath the Iranian micro-continent (e.g., Walpersdorf et al., 2014; Burg, 2018).

In the recent decades, different parts of the Arabia-Eurasia convergence zone were studied in detail; the pieces of the puzzle of this convergence are progressively fitting together. Numerous studies have attempted to describe the role of strike-slip faults in the active tectonics of the collision zone (e.g., Hessami et al., 2003; Karakhanian et al., 2004; Talebian and Jackson, 2004; Walker and Jackson, 2004; Regard et al., 2005, 2006; Authemayou et al., 2006; Meyer and Le Dortz, 2007; Shabanian et al., 2009a, 2009b and 2012a; Molnar and Dayem, 2010; Farbod et al., 2011, 2016; Calzolari et al., 2015, 2016, 2018). According to these studies, strike-slip faults play significant roles in the current deformation of the Iranian plateau and were responsible for several moderate to large earthquakes especially in east of Iran (e.g., Dasht-e Bayaz 31 August 1968, Koli-Buniabad 27 November 1979 and Zirkuh-Qayen 10 May 1997). Since Pliocene (5.3-2.6 Ma), the dominant tectonic regime in the Iranian plateau and surrounding deformation belts has changed from compressional to strike-slip (Regard et al., 2005, 2006; Authemayou

et al., 2006; Shabanian et al., 2009a, 2009b, 2010; Farbod et al., 2011, 2016; Ghods et al., 2015; Tadayon et al., 2017, 2018; Taghipour et al., 2018). Even in thrust-fold domains such as the Zagros and Alborz belts, where the main way of accommodation of Arabia-Eurasia convergence is crustal shortening, the role of strike-slip faulting is determinant (e.g., Talebian and Jackson, 2004; Authemayou et al., 2006, 2009).

The role of major strike-slip faults such as the North Tabriz Fault in northwest Iran (e.g., Cisternas and Philip, 1997; Karakhanian et al., 2004; Ghods et al., 2015), the Main Recent Fault in Zagros (Tchalenko et al., 1974; Braud and Ricou, 1975; Ricou et al., 1977; Berberian, 1995; Talebian and Jackson, 2004), the Minab-Zendan-Palami fault zone at the Zagros – Makran transition (Regard et al., 2005) and the Bakharden-Quchan fault system in Kopeh Dagh (Shabanian et al., 2009a, 2009b) as well as the faults that re-activate the Sistan Suture zone in the east of Iran (e.g., Vernant et al., 2004; Walker and Jackson, 2004) in accommodation of the Arabia-Eurasia convergence is nearly well-known. These strike-slip faults act as block boundaries along which the blocks are moved in accordance with the overall deformation in the Arabia – Eurasia collision zone (e.g., Walpersdorf et al., 2006, 2014; Tavakoli et al., 2008; Shabanian et al., 2009b; Mousavi et al., 2013; Ghods et al., 2015).

Recent geodetic (e.g., Vernant et al., 2004; Reilinger et al., 2006; Mousavi et al., 2013; Walpersdorf et al., 2014) and geological studies (Shabanian et al., 2009a, 2009b, 2010, 2012b; Farbod et al., 2011, 2016) in NE Iran have revealed that active deformation is localized along block-bounding crustal faults. In Central Iran, GPS-derived velocity fields (Walpersdorf et al., 2014) and GPS block modeling (Reilinger et al., 2006; Walpersdorf et al., 2014) show that about 90 percent of the 5.7 mm/yr northward motion of the Lut block – Eurasia is transferred to the north of the E-W Doruneh fault (Fig. 1). To the north, the Bakharden-Quchan fault system takes up 4.1 - 4.6 mm/yr of this dextral faulting across the Kopeh Dagh Mountains (Shabanian et al., 2009a, 2009b, 2012b; Mousavi et al., 2013). In other words, this fault system accommodates 80% of Central Iran-Eurasia convergence (~5.1 mm/yr) north of 37°N. In this tectonic context, there are other strike-slip faults such as the Doruneh and Dasht-e Bayaz faults which affect the Iranian plateau and are characterized by conspicuous seismic and/or geological

activities. Nevertheless, the role of these faults in the accommodation of the active convergence has been a matter of debate (e.g., Farbod et al., 2011, 2016; Nozaem et al., 2013; Calzolari et al., 2015, 2016, 2018; Tadayon et al., 2017 and 2018). Interestingly, these E-W faults are perpendicular to the N-S active block motions in the Lut and separate the N-S dextral strike-slip faults of the Lut borders (the Nayband and Sistan suture zone) to the south from the NW-trending structures of the Binalud and Kopeh Dagh deformation domains to the north (Fig. 1).

Our understanding of the processes involved in the plate convergence improves progressively, but we still need to know more about (1) both the pattern and kinematics of deformation in each part of the convergence/collision zone and (2) the role of intracontinental crustal faults in the accommodation of this deformation within the plateau. During the last century, areas such as Dasht-e Bayaz, Tabas, and Bam that were considered as stable areas in the interior of rigid blocks have been affected by large destructive earthquakes occurring on mostly unknown faults (e.g., Walker et al., 2011; Berberian, 2014). After the destructive 1968 Mw 7.1 earthquake, for instance, the Dasht-e Bayaz area has been one of the most seismically active domains in Iran. Right after the Dasht-e Bayaz main shock in 1968, this area has been studied from different points of view. The first studies focused on mapping of the coseismic rupture and post-earthquake observations (e.g. Ambraseys and Tchalenko, 1969; Tchalenko and Ambraseys, 1970; Tchalenko and Berberian, 1975). Meanwhile, more recent studies have focused on the seismology and the active tectonics of Dasht-e Bayaz and surrounding areas in the context of Arabia-Eurasia convergence (Walker et al., 2004; Walker and Jackson, 2004; Walker et al., 2011). However, the main unanswered question regards the role of the E-W sinistral faults such as the Dasht-e Bayaz fault in accommodation of the NNE Arabia - Eurasia convergence (e.g., Vernant et al., 2004; Walpersdorf et al., 2014) between Central Iran and Eurasia. This question can be answered partly through an investigation of the temporal and spatial kinematic evolution of the Dasht-e Bayaz fault and its kinematic interaction with other major structures including the Sistan suture zone. It is also important to know whether the stress field in eastern Iran is due to the stress transfer from the Arabia – Central Iran collision, or is influenced by the geometry and relative motion of individual blocks in eastern Iran (e.g., Jentzer et al., 2017).

This paper especially focuses on the Pliocene-Quaternary to present-day states of stress (the last 5 Ma) in the region affected by the Dasht-e Bayaz fault (Fig. 1); the paleo-tectonic evolution of the area is of course out of the scope of this study. We applied the inversion technique on both kinds of fault slip data as provided through focal mechanism of earthquakes and fault measurements in the field, with well-known senses and relative chronologies. The level of consistency of our results has been discussed in the light of previous studies on the Cenozoic stress field of the Iranian plateau and surrounding deformation belts. We have then put our results in a larger framework, which we have reconstructed using available kinematic data and results from the east and northeast Iran. This has allowed us to discuss the possible interaction of the Dasht-e Bayaz fault with other active faults of the region. Finally, we have proposed a kinematic scenario to describe the role of strike-slip faulting in the accommodation of active convergence in ENE Iran.

2. Geodynamic and seismotectonic framework

According to geological investigations (e.g., Berberian et al., 1999; Walker and Jackson, 2004; Mayer and Le Dortz, 2007; Foroutan et al., 2014) and geodetic Global Positioning System (GPS) measurements (e.g., Vernant et al., 2004; Walpersdorf et al., 2014), the N-striking right-lateral faults in Central Iran, especially on both sides of the Lut block (Fig. 1), accommodate the northward motion of Central Iran relative to Eurasia (Helmand block in Afghanistan). The Distribution of historic records and instrumental earthquake epicenters, as well as the GPS velocity field show that the convergence is mainly accommodated along the block boundaries, while the interior of the blocks (e.g., Lut block) is almost rigid (e.g., Vernant et al., 2004; Walker and Jackson, 2004; Walpersdorf et al., 2014), with low rates of deformation. The crustal-scale dextral shear continues up to the latitude 34°N, north of which E-W left-lateral faults like the Dasht-e Bayaz, Niazabad and Doruneh (further north) are present (Fig. 1). At this latitude, the change in geology is accompanied by a change in active faulting from the N-S dextral faults of the Sistan suture zone to a system mainly constituted by E-W sinistral strike-slip faults (e.g., Berberian

et al., 1999). The role of these crustal faults in the accommodation of active deformation perpendicular to the N-S dextral shear has been a matter of debate since, at least, thirty years ago (e.g. Jackson and McKenzie, 1984; Berberian et al., 1999; Walker and Jackson, 2004; Farbod et al., 2011, 2016; Aflaki et al., 2019). The recent works by Nozaem et al. (2013), Calzolari et al. (2015 and 2016) documented Neogene to Quaternary dextral strike-slip deformation along the NE-SW Kuh-e-Sarhangi and the E-W Kuh-e-Faghan faults and have revealed another complexity in the active kinematics of northwest Lut – Central Iran (Fig. 1). The objective of this part is a brief demonstration of the structural schema and the seismotectonic activity of an active fault network, with complex internal interactions; for this reason we only selected some of the most important and crucial seismic activities in the area without pointing out other subsidiary events that have not been assigned to particular faults.

Active tectonic and seismological studies conducted in Dasht-e Bayaz and the surrounding areas documented that the active faults, responsible for numerous seismic shocks in the area, are temporally and mechanically in close interaction (e.g., Berberian et al., 1999; Walker et al., 2004; Walker et al., 2011). On 31 August 1968, a tremendous destructive earthquake (Mw 7.1) shocked the area and produced a 70 km E-W coseismic rupture; the maximum coseismic displacement (4.5 m left-lateral and 2.5 m vertical) was measured in north of the Nimboluk plain (Tchalenko and Ambraseys, 1970; Tchalenko and Berberian, 1975). The formerly called Dasht-e Bayaz fault was renamed later as the western segment of a now longer Dasht-e Bayaz fault, subsequent to the reactivation of its 55 km length extension to the east. The eastern segment of the Dasht-e Bayaz fault with the same trend and straight geometry attracted attention after 27 November 1979 Mw 7.1 Koli-Buniabad earthquake, only 11 years after the Dasht-e Bayaz main shock (e.g., Berberian et al., 1999).

The most remarkable seismic events occurred just 20 hours after the Dasht-e Bayaz main shock during the Ferdows earthquakes of 1st and 4th September 1968 (Mw 6.3 and Mw 5.5, respectively) about 70 km west of the Dasht-e Bayaz village. The close proximity (or even overlap) between the domains of impact of the Dasht-e Bayaz and Ferdows earthquakes has prevented researchers from separating their field effects (e.g., Berberian, 2014). Several authors, based on field observations, suggested that the two

earthquakes occurred on the NW–trending Ferdows reverse fault (Figs. 1 and 2); the reverse focal mechanisms of the earthquakes were also compatible with this fault (see Berberian, 2014 and references therein). After 11 years and during less than one month, three other destructive earthquakes of Korizan (14.11.1979), Koli-Buniabad (27.11.1979 - e.g., Haghipour and Amidi, 1980) and Kalateh Shur (07.12.1979 - e.g., Haghipour and Amidi, 1980; Ambraseys and Melville, 1982) occurred along the northern part of the Abiz fault, the eastern segment of the Dasht-e Bayaz fault and at the intersection of the two faults, respectively. The Zirkuh earthquake of 1997 May 10 (Mw 7.2), caused by the northern segment of the NNW-striking Abiz fault (Fig. 1), has also been considered as the sequence of seismic events triggered by the Dasht-e Bayaz main shock on 31 August 1968 (e.g., Berberian et al., 1999). The 125-km-long surface faulting which, with dextral strike-slip mechanism has occurred during the Zirkuh earthquake is known as the longest surface rupture associated with an Iranian earthquake (e.g., Berberian et al., 1999). This NNW-striking fault segment changes into a NNE-SSW strike (causative fault of the November 14, 1979 Korizan earthquake; see above) near the eastern end of the Dasht-e Bayaz fault and provides its dextral pair of a conjugate-like arrangement (see section 4; Fig. 3A).

The 1968, 31 August earthquake of Dasht-e Bayaz is considered as a trigger for the reactivation of the east segment of the Dasht-e Bayaz fault, the Ferdows reverse fault zone and the Korizan fault, causing a sequence of earthquakes (e.g. the Zirkuh, Koli-Buniabad and Ferdows earthquakes). The 1968.09.11, 1979.01.16 and 1997.06.25 events did not rupture the surface (e.g. Berberian et al., 1999). The 1979.01.16 event showed NW-striking reverse faulting and 1997.06.25 event has produced both the possibilities of N-S right-lateral or E-W left-lateral faulting (Berberian et al., 1999). The calibrated relocations and the body-wave modeling of Walker et al. (2011) showed that the epicenter of the 1979.01.16 earthquake is centered on an SW–dipping reverse fault. As for the 1997.06.25 event, Walker et al. (2011) also proposed that, through InSAR results, the rupture had occurred on the N–S trending dextral fault plane without the possibility to attribute it to any of the Boznabad or Pavak faults (Fig. 2).

Based on this seismicity, it is concluded that the Dasht-e Bayaz and nearby faults are in close kinematic interaction to accommodate the active deformation of the area. This sequence of the Dasht-e-

Bayaz, Ferdows and Zirkuh earthquakes (occurred between 1968 and 1997) presents one of the most remarkable examples of temporally clustered continental seismicity in the world (e.g., Berberian et al., 1999; Walker et al., 2011). These consecutive destructive earthquakes could have been triggered by the 31 August 1968 Dasht-e Bayaz main shock (e.g., Berberian et al., 1999 and references therein) and occurred along the faults with different kinematics.

3. Methodology

3.1. Inversion of fault-slip data

Following the method proposed by Carey and Brunier (1974), determination of a deviatoric stress tensor from fault slip data is based on the stress-slip relationship described by Wallace (1951) and Bott (1959). Computer programs, developed for the inversion of fault slip data, compute a mean best fitting deviatoric stress tensor from a group of striated fault planes by minimizing the angular deviation (misfit angle) between the observed striation and the shear stress resolved on the fault plane (Carey and Brunier, 1974, Carey; 1979; Angelier, 1990). The inversion results are revised and refined iteratively to reach the smallest misfit angle while involving the highest possible number of measured homogenous fault slip data. The meaningful process of stress determination (deviatoric reduced stress tensor) from both geological and seismological fault slip data is a delicate challenge requiring good quality of data, meticulous observations and data separation as well as adequate knowledge on both kinematics and mechanics of faulting (see Allmendinger et al., 1989; Shabanian et al., 2010; Hippolyte et al., 2012; Tranos, 2018). A blind use of abundant computer programs (whatever the software is used) seems very simple, but it would lead to mathematic results without geological significance (see Hippolyte et al., 2012 and Tranos, 2018 for details).

The method we used is principally invented (Carey and Brunier, 1974; Carey-Gailhardis and Mercier, 1987) for the analysis of multiphase heterogeneous fault slip datasets measured in natural fault

outcrops which contain a variety of new created and preexisting fault planes reactivated in distinct stress states. This method easily works with both new created conjugate fault pairs and preexisting faults with unknown geometric relationships and is independent of conjugate fault arrangements for resolving reduced stress tensors (see Carey-Gailhardis and Mercier, 1987 and 1992; Bellier and Zoback, 1995; Regard et al., 2005; Shabanian et al., 2010 for more details). As a main aspect of the program we have used (i.e., FCALC – Geodyn-Soft; Carey-Gailhardis and Mercier, 1987), there is no way for automatic separation of fault slip data and this job have to be done through detailed geological field observations and individual notes on the quality, reliability and chronological relationships (cross-cutting or overprinting) of the structural elements measured in the field, as well as mechanical compatibility of the fault slip data to the resolved stress tensor. Interestingly, the well-known misfit angle, which is an essential criterion for the computer software during the iteration and minimization processes, is the last parameter we consider for the analysis of a heterogeneous fault dataset. This considerably reduces the effect of geologically incompatible slip data in resolving a deviatoric stress tensor. This is simply because an apparently homogenous dataset (separated without reliable geological considerations) could be synthesized through optimizing the misfit angle distribution of the stress model and an arbitrary selection of data mainly based on this criterion. While, that dataset could comprise fault slip data which in reality belong to different tectonic regimes but apparently are compatible with an artificial mean stress tensor resolved from marginal data from those different datasets. Therefore, the misfit angle only shows the level of compatibility of data with a given stress model regardless its geological reliability!

Principal inputs are fault-slip data from geological faults measured in the field or seismologically determined focal mechanism of earthquakes including attitudes (e.g., strike/dip/dip quadrant) of striated fault planes and associated striations with well-known sense of movement. As a great advantage, acquisition of field data is feasible almost everywhere and a careful inversion analysis of good quality fault slip data, with known chronological relationships, would lead to a reliable reconstruction of the kinematic history of an area (e.g., Angelier, 1984; Carey-Gailhardis and Mercier, 1992; Hippolyte et al., 1993; Bellier and Zoback, 1995; Regard et al., 2005; Shabanian et al., 2010). The main outputs of this

method are orientations (trend and plunge) of principal stress axes σ1≥ σ2≥ σ3 (corresponding maximum, intermediate and minimum stresses, respectively) and "R= (σ2-σ1)/(σ3-σ1)". This linear parameter (R) equals 1−φ, φ being another commonly used stress ratio (e.g., Angelier, 1979; Zoback, 1989; Ritz and Taboada, 1993), and describes relative stress magnitudes ranging from 0 to 1 (e.g., Carey and Brunier, 1974; Mercier et al., 1991; Bellier and Zoback, 1995, Shabanian et al., 2010 and references therein). Different combinations of Andersonian stress arrangements (vertical principal stress axes of σ_1, σ_2 and σ_3 for pure extensional, strike-slip and reverse faulting, respectively) and R values lead to various stress regimes responsible for different kinds of faulting (see Ritz and Taboada, 1993; Shabanian et al., 2010 for more details). We used the method originally proposed by Carey (1979); the results deduced from inversion of fault-slip data measured in individual sites along the Dasht-e Bayaz fault and nearby areas are presented in Table 1 (see Figs 3 and 9 for site locations).

3.2. Relative chronology of fault slip data and data separation

According to an important assumption accepted in fault kinematic inversion methods, a distinct stress tensor (σ1≥ σ2≥ σ3 and "R") can create only one slip direction on a given fault plane. The complications of data separation are normally revealed when different sets of heterogeneous fault-slip data are collected from fault planes. Several generations of striae on a single fault plane are surely the result of changes in angular relationships between the fault plane and principal stress axes. Nevertheless, the nature of such changes could either be (1) due to temporal variations in the stress field or (2) could imply the rotation of the fault plane during deformation. In both cases, the chronology of striae is usually determined through the crosscutting relationships of striations and/or fault planes complemented by geological field observations. Except for some probable mistakes in measurements and individual cases of local rotations due to progressive deformation, the fault slip data are usually classified into homogenous sub-groups. In some of related studies, the automatic or semi-automatic methods have also been proposed or utilized to separate heterogeneous fault slip data (e.g., Nemcok and Lisle, 1995; Salvini and

Storti,1999; Fry, 1999; Rossetti et al., 2002; Shan et al., 2003; Tranos, 2015, 2018), however, in this study we preferred to take advantage of techniques concerning data separation based on geological observations and kinematic rules (see Shabanian et al., 2010). Figure 8 shows an example of this strategy which is based on crosscutting relationships, field observations and kinematic considerations. The 10 measurement sites were chosen in outcrops of different stratigraphic ages, ranging from Triassic to Quaternary (Figs 3 and 10); almost half of the measurements (a total number of 170 fault slip data) were done on fault planes affecting Pliocene and Quaternary deposits (see Table 1). Relative chronologies of different generations of striations on a fault plane or in a outcrop has been determined based on the superposition of striations and/or crosscutting relationships between fault planes affecting the outcrop. In a given outcrop, usually, there are few fault planes showing direct chronological indicators for different generations of striations, while the majority of planes only express one direction of striation with unknown relative chronology (see Shabanian et al., 2010 for more details). In such the case, fault slip data of different generations have primarily been separated using the well-known relative chronologies observed in the field and then, other compatible fault planes with only one striation were added to each data set based on their kinematic and mechanical compatibilities with the data set, as well as the geological field notes on each fault plane (Fig. 8). The final chronology of the resolved deviatoric stress states (defined as paleo, intermediate or modern stresses) has been determined considering the age of youngest rock units affected by each stress state and chronological cross-relations between different stress tensors.

Certain criteria should be met in order to determine reliable stress solutions (e.g. Etchecopar, 1984; Carey-Gailhardis and Mercier, 1992; Belier and Zoback, 1995; Shabanian et al., 2010): (1) we need at least 4 fault planes with different attitudes that are well-distributed in the space. A higher number of fault planes and a good spatial distribution will result in a more constrained stress solution, (2) the inversion results will theoretically be reliable when at least 80 percent of deviation angles are under 20°, that means a confidence level of 68 per cent in a Gaussian probability distribution (3) the measured fault planes must show good mechanical compatibility with the stress tensor solution. For instance, a set of transtensional faults cannot be explained by a compressional stress tensor even if output parameters of the tensor to be

281 excellent, (4) a reliable stress solution needs fault slip data of good quality; it greatly depends on the
282 details of field observations, the tectonic history of the measurement site and user's experiences of data
283 measurement and inversion analysis. Considering these criteria, A, B and C were assigned to well-
284 constrained, constrained and poorly-constrained stress tensor solutions, respectively. For solutions from
285 less than four well-distributed fault planes, we used a fixed solution (Bellier and Zoback, 1995) in which,
286 one principal stress axis is fixed as vertical. In this study the quality of fixed solutions has been
287 considered the same as C and they were marked as CF; the stress ratio "R" is not valid for this kind of
288 solutions.

289 According to the abovementioned method, the measured fault slip data were separated into three
290 homogeneous groups of slip generations and were analyzed. This analysis has provided basic information
291 for describing the last kinematic evolution of the Dasht-e Bayaz fault during the Pliocene and Quaternary
292 times. We compared the pattern of kinematic changes along the Dasht-e Bayaz fault with similar studies
293 in nearby regions in E and NE Iran (e.g. Shabanian et al., 2010; Farbod et al., 2011; Javidfakhr et al.,
294 2011; Jentzer et al., 2017; Tadayon et al., 2017), which has allowed us to place our results in a larger
295 geodynamic scale (see the discussion).

296

297 **3.3. Inversion of earthquake focal mechanism data**

298 We determined the present-day state of stress in the Dasht-e Bayaz area through the inversion of
299 focal mechanisms of medium to large (7.1>M>5.5) earthquakes applying the method described by Carey-
300 Gailhardis and Mercier (1987). These earthquakes have occurred between 1968 and 1997 comprising the
301 Dasht-e Bayaz main shocks. We have only used focal mechanism solutions that had been relocated and
302 modeled using body waves by Walker et al. (2004, 2011). With this method, we analyzed two orthogonal
303 nodal planes for each earthquake focal solution taking into account that only one plane was reactivated
304 during the earthquake due to the regional stress state. The final selection among each pairs of nodal planes
305 can be done by (1) direct observation of the surface rupture of the earthquake, (2) seismological

investigations of the rupture process, (3) the spatial distribution of aftershocks and (4) the inverse computation by selecting the nodal plane that results in greater consistency with the regional stress field (Carey-Gailhardis and Mercier, 1987). For determining the regional state of stress, the importance of the main shocks (even a single datum) is significantly greater than that of the aftershocks because small earthquakes would probably reflect kinematic instabilities due to heterogeneous deformation and independent faulting in small-scale bodies (e.g. Carey-Gailhardis and Mercier, 1992). For some of the main shocks, we have direct information on the rupture geometry from field observations (Tchalenko and Ambraseys, 1970; Berberian et al., 1999). This serves as a reference for evaluating the compatibility (in a geometric sense) of other events using inverse computation. This method was successfully applied to determine the causative fault plane of the second event of August 2012 earthquake doublet (Mw 6.4, 6.2), that had occurred in the Ahar-Varzaghan complex fault system in NW Iran (see Ghods et al., 2015 and Momeni and Tatar, 2018).

3.4. Active fault mapping

During the four last decades, several studies have focused on different aspects of the Dasht-e Bayaz earthquake fault providing structural maps of the fault at different scales and at distinct aims (e.g., Tchalenko and Ambraseys, 1970; Tchalenko and Berberian, 1975; Walker et al., 2011). However, the specific scope of our study on kinematic aspects of the fault and its interaction with other neighboring main faults has led us to prepare a detailed fault map using the high resolution satellite images (Bing images in SAS Planet, http://sasgis.org; 1 m resampled pixel size) of the area. A simplified version of this map is shown in Figure 3, while the more detailed maps are centered on the fault terminations and intersection zones (Figs 4-7), where additional information are needed to describe the structural characteristics of the Dasht-e Bayaz fault. Thanks to our new fault mapping, we reinterpreted the structural relationships between the main fault and other structures interacting with from the eastern termination westwards along the Dasht-e Bayaz fault (see below).

4. Active tectonics and structure of the Dasht-e Bayaz fault

The Dasht-e Bayaz fault is a 120-km-long sinistral fault in the north of the Lut block (Fig. 1). The E-W Dasht-e Bayaz fault, with an almost straight geometry, is a structural assemblage of several fault strands with different orientations ranging from N070°E to N110°E (e.g., Tchalenko and Ambraseys, 1970; Fig. 3). This particular structural arrangement forms various contractional and extensional mesoscale structures and the associated morphotectonic landforms such as pull-apart basins, pressure ridges and en-echelon folds at different scales along the fault zone; the same structural patterns were seismically created during the 31 August 1968 Dasht-e Bayaz main shock (Tchalenko and Ambraseys, 1970; Berberian et al., 1999). In addition to these variations in the fault geometry, the Dasht-e Bayaz fault is affected by N-S dextral faults which are in close interaction with the main fault (Figs 3 and 4).

At the eastern end, the Dasht-e Bayaz fault intersects the NNE-striking Korizan segment of the Abiz fault (Fig. 3). As an important verified observation, north of 34°N, it is difficult to define any relative dominance for the N-S Korizan or the E-W Dasht-e Bayaz faults while south of this latitude, the N-S dextral faults are dominant and cut both the E-W sinistral and the NW-SE reverse faults of the region (e.g., Berberian et al., 1999). Near the village of Buniabad in the south of Kheybar Kuh-e Kuchek (i.e., Little Kheybar Mountain), these faults join together into a single ENE-WSW trend (Fig. 3). Farther northeast, however, the sinistral Niazabad fault runs parallel to the Dasht-e Bayaz fault and looks like a left-hand stepping segment in a larger E-W sinistral fault system (Fig. 1), which is apparently dominating the N-S dextral fault system of the Sistan suture. The northern parts of the Korizan fault are partly covered by eolian deposits, while the overall fault trace in the south of Buniabad village (Fig. 3) cuts the Quaternary alluvial fan surfaces. Our mapping of the intersection area shows a deforming wedge between the main traces of the Dasht-e Bayaz and Korizan faults (Fig. 3a); the conjugate arrangement of the main faults implies active contraction inside the wedge. Interestingly, N-S fault traces appear again in a discontinuous way in the northern side of the Dasht-e Bayaz fault trace, cutting through Kheybar Kuh-e

Kuchek. Except for a few places (see Walker et al., 2011), the N-S fault strands cut the bedrock and there is no way to evaluate their Quaternary activity. Nevertheless, systematic dextral geomorphic offsets of main streams along these faults could indicate their activity during, at least, the Pliocene time.

Another structural node along the Dasht-e Bayaz fault occurs where it intersects with the N-S Mahyar fault (Fig. 4). In fact, the Mahyar fault (e.g. Berberian, 2014) separates the western and eastern earthquake segments of the Dasht-e Bayaz fault (ruptures of the 31 August 1968 and 27 November 1979 earthquakes, respectively). Our detailed mapping of the intersection area (Fig. 4) shows that the cross-cutting dextral Mahyar fault and the sinistral Dasht-e Bayaz fault form a typical crosswise (nearly orthogonal) fault arrangement in the middle part of the Dasht-e Bayaz fault trace. These coexisting faults have displaced each other in the sense of their movement of about 1.5 km (Figs 3 and 4). Following the opposite shear senses of the crosswise faults, double-coupled extensional and contractional domains have been formed in the quarters of this intersection. In the NW and SE extensional quarters, there are two relatively lowlands with an average elevation of 1300 m, while the adjacent NE and SW contractional quarters occupy higher areas with the average elevation of 1400 m (Fig. 4). The NE contractional quarter is occupied by nearly E-dipping reverse faults which join the main trace of the eastern Dasht-e Bayaz fault, southwards (Fig. 4).

In the same area, around the Dasht-e Bayaz and Mahyar faults intersection zone (Fig. 4), different sets of dioritic and andesitic dikes have intruded in folded rocks of Jurassic to Eocene ages (Alavi Naini and Behruzi, 1983; Fauvelet and Eftekhar-Nezhad, 1991). Pliocene deposits cover these post folding dikes and define their stratigraphic age of post Eocene – pre Pliocene. We have mapped 379 dikes through the analysis of Bing Map (SAS Planet©) satellite images of the area. The clear crosscutting relationships of the dikes show three generations of which the oldest set (microdioritic dikes; Mohammadi Gharetapeh et al., 2014) is the most frequent, with a dominant orientation of N330±10°E (Fig. 4). Two younger minor populations of dikes (pyroxene andesitic with N345±15°E and N10±10°E preferred orientations) are less abundant in the area and clearly cut through the oldest generation where coexisted.

Our new mapping of the 1979 earthquake rupture reveals that the main trace of the coseismic rupture dies out westward into a N-S reverse fault zone, with a dextral component of faulting (Figs 4 and 5). Other parallel reverse/thrust faults are observed in this quarter, but those haven't been picked up by the coseismic rupture (Fig. 5). In contrast, the adjacent NW extensional quadrant hosts the extensional termination of the 1968 coseismic rupture (Fig. 5). In this area, the E-W trend of the 1968 rupture dies out eastwards into a NE-striking normal fault zone of which a 615-m-long array of surface rupture can be mapped in recent satellite images (Figs 4 and 5). The alignment of several SE-facing landslides (with fresh free-faces recognizable on images) along this part of the rupture is coherent with the extensional character of the rupture termination.

Farther west, the Dasht-e Bayaz fault reaches an E-W, pull-apart basin (the Chah Deraz pull-apart basin), which possesses an elongated shape (~3900 m in length and ~870 m in width), with the length to width ratio of 4.5. The almond-shaped geometry of the pull-apart basin, in addition to its symmetric curved boundaries (Fig. 6) implies that the basin was formed in a releasing bend (e.g., Dooley and Schreurs, 2012) along the Dasht-e Bayaz fault. Considering the lack of Quaternary activity along the southern border of the basin and the coseismic reactivation of the northern master fault during the 31 August 1968 earthquake (Fig. 6), we suggest that the pull-apart basin has entered a new stage of evolution, by a shift in active extension from the central part to the northwest margin of the basin (Fig. 6).

Further to the west, the Dasht-e Bayaz fault controls the contact between Quaternary deposits and Mesozoic sedimentary rocks. In the north of Nimboluk plain, there are outcrops of Miocene marls armored by Quaternary deposits; the dense cultivation and human-made changes in the Quaternary surfaces, cut by the fault, precluded us from following the trace of the coseismic rupture. The detailed rupture maps of Tchalenko and Ambraseys (1970) and Tchalenko and Berberian (1975) show that about 12 km westwards from the Chah Deraz pull-apart, the fault trace encounters another structural complexity (Fig. 7). After a 5-km-long en-echelon fracture zone, the main rupture trace turns southwest and continues to the west for ~20 km. This coseismic fault rupture (Mozdabad fault branch) crosses between Dasht-e Bayaz and the Khezri villages and, in the southwest of Mozdabad village, it joins the Ferdows reverse

fault array at the western flank of the Kuh-e Kamarkhid and Kuh-e Kalat mountains (Figs. 2 and 3). Interestingly, the main fault trace, visible in the geomorphology of Quaternary alluvial fans, can be directly traced to the west of the Chah Deraz segment, while only a small part of this Quaternary fault has been reactivated during the 1968 earthquake. This branch of the Dasht-e Bayaz geologic fault continues westwards for 13 kilometers, where it bends towards the northwest and joins the north dipping reverse faults in the middle of Kuh-e Kamarkhid (Fig. 2 and 7A). In that area, a series of en-echelon pressure ridges and folds have been formed due to a restraining curvature along the Dasht-e Bayaz fault (Fig. 7).

In summary, our new detailed mapping of the Dasht-e Bayaz fault trace and the related structures (thanks to the available very high resolution satellite images and other facilities) reveals that the Dasht-e Bayaz fault is a complex fault zone in which several fault strands with different orientations and kinematics are actively interacting. In this context, N-S dextral and E-W sinistral faults play a significant role in both the structural pattern and active tectonic deformation along the main fault zone.

5. Fault kinematics and states of stress in the Dasht-e Bayaz area

5.1. Modern state of stress

The analysis of the youngest group of fault slip data were measured in ten sites (Table 1, Figs 9 and 11) including the last coseismic kinematics of the Dasht-e Bayaz fault (for example, sites 2, 5 and 6 in Figs 10a, 10e-f and 10h, respectively). Except for sites 4, 5b and 6, the maximum stress axis (σ_1) has the average trend of N045±5°E (Fig. 13C) and the deviatoric stress tensors indicate a homogenous strike-slip stress field in the area including the Dasht-e Bayaz fault (Figs 9 and 11). The trend of the σ_1 axis locally changes in sites 5b, 6 and 4, with an orientation of ~N070°E (see the section 6.1 for more details).

To avoid local stress changes caused by structural rotations in fault zones and local stresses produced at structural complexities such as fault bends, fault relay zones and fault-bend terminations, we have analyzed together the youngest set of fault-slip data only from main fault planes (MFP) measured

over the study area (Figs 10 and 11). A main fault plain is the most prominent structure which controls overall deformation in a given outcrops (for instance, fault planes marked in Figs 10a, 10c, 10f- j) and is usually distinguished from other subsidiary fault planes in the outcrop during field measurements. The inversion analysis of such a particular data set leads to a mean regional stress state responsible for the reactivation of different main fault planes regardless their geographic location and structural setting. The resulting stress tensor specifies a mean regional strike-slip stress regime characterized by a N42±05°E σ_1 axis (Fig. 11). This regional mean σ_1 axis is very close to the average orientation of N45±05°E for the σ_1 that we have independently obtained in 8 individual sites (Fig. 14C). Almost all the stress tensors (except for sites 5A, 6 and 7) were resolved from the analysis of strike-slip fault planes, with pitch angles less than 20° (Fig. 11), showing different dextral or sinistral dominant component of faulting in accordance with their orientation with respect to the principal stress axes (Fig. 11). This strike-slip character is also consistent with the regional mean stress tensor deduced from the inversion of main fault planes (MFP in Fig. 14) and is confirmed by the mean R value of ~0.54 for the tensors with Andersonian strike-slip arrangement (Fig. 11 and Table 1). Accordingly, a prominent pure strike-slip regime is representative for the modern stress field over the study area.

5.2. Paleostress state

In 8 sites along the Dasht-e Bayaz fault, we have observed signatures of the oldest generation of fault slip data. These older data, which were naturally fewer than the younger data, were carefully differentiated and analyzed regarding both our field observations and cross-relation of different individual data in each site. For example, our filed observation in site 7 indicates the signature of two distinct deformation stages in Neogene deposits (Figs 8 and 12). A total number of 20 fault planes were measured in site 7. The SE-striking fault planes show an older dextral reverse kinematics (striation 1 in Fig. 8) overprinted by a younger pure reverse kinematics (striation 2 in Fig. 8). The younger fault slip data set is compatible with the modern stress state, while the older data set defines an older reduced stress tensor

457 characterized by a NW-trending maximum compression (Fig. 8C). E-W planes in this data set are
458 oblique-slip dextral reverse faults (right-hand stereogram in Fig. 8C).

459 In six of eight sites, which are well distributed over the study area, the oldest data sets comprise
460 sufficient data to give independent deviatoric stress tensors (Figs 9 and 12; Table 1). These individual
461 stress tensors represent a paleostress state characterized by a homogeneous N135±15°E trending mean σ_1.
462 As for the dominant stress regime, except for two stress tensors resolved for sites 6 and 7, the other
463 tensors are fixed solutions, with less than four differently oriented fault planes (see the methodology
464 section). In this case, the tensors cannot be used for determining the stress regime. However, the majority
465 of fault planes analyzed in these paleostress tensors is oblique-slip with a dominant reverse component
466 (Fig. 12) and are coherent with a transpressional stress regime as indicated by the B-Quality tensor 7 in
467 Figure 12. In this paleostress regime, the E-W fault planes, which were measured on the earthquake fault
468 trace of Dasht-e Bayaz or on other faults parallel to it, are oblique-slip reverse dextral faults and show a
469 transpressional character (Fig. 8d).

470

471 **5.3. Intermediate state of stress**

472 In addition to these paleo and modern states of stress, the signature of an intermediate stress field
473 was also measured in three sites along the Dasht-e Bayaz fault (Figs 8, 13; Table 1). This intermediate
474 stress is characterized by a ~N009°E mean σ1 and a strike slip stress regime (Fig. 14B). However, the
475 insufficient number of stress solutions for this stress state precludes us considering it as an independent
476 regional stress field (see the discussion).

477

478 **5.3. The present-day state of stress deducted from inversion of earthquake focal mechanisms**

479 We have used 15 earthquake focal mechanisms that have been recorded in the Dasht-e Bayaz and
480 nearby areas and have been modeled by Walker et al. (2004, 2011) using body wave modeling (Table 2).
481 The final stress tensor was resolved through the inversion of fault slip data from several earthquakes

affecting a vast area around the Dasht-e Bayaz fault and is therefore representative of the present-day regional state of stress in the northern Lut block. This solution indicates a single strike-slip tectonic regime, which characterized by a regional N050±05°E trending σ_1 (Fig. 15) responsible for the active deformation (whatever reverse or strike-slip fault mechanism) throughout the region.

6. Discussion

6.1. Regional versus local stress changes in the Dasht-e Bayaz and close vicinity

In this study, the spatiotemporal changes in the state of stress were investigated through the inversion of fault slip data measured in ten sites along the Dasht-e Bayaz fault. Based on the inversion of independent sets of geologic fault slip data (a N045±05°E compression with strike-slip regime) and earthquake focal mechanisms (a single strike-slip tectonic regime, with a regional N050±05°E trending σ_1), the present-day state of stress in the Dasht-e Bayaz area is characterized by a mean regional N050±05°E trending σ_1 accommodated by strike-slip tectonics (Fig. 15). The consistency of these results reveals (1) the absence of remarkable change in the modern state of stress during the late Quaternary time, (2) the prevalence of a homogeneous stress field in the brittle crust (above the ~17 km depth of seismogenic layer) of the Dasht-e Bayaz region and (3) the lack of stress perturbation due to the activity of the Dasht-e Bayaz fault.

The main strike-slip stress regime deduced along the eastern and middle parts of the Dasht-e Bayaz fault changes into a compressional stress regime at the western end of the fault (sites 6 and 7 in Figures 9 and 11). These two distinct stress regimes are coherent with different structural settings of the resolved stress tensors. In fact, despite the strike-slip character of the fault that is clearly expressed along its eastern and central portions (e.g., Tchalenko and Ambraseys, 1970), the kinematics of the Dasht-e Bayaz fault changes to oblique-slip sinistral reverse at its western end. In this area, the strike-slip character of the Dasht-e Bayaz fault disappears near the NW-SE Ferdows thrust (Berberian, 1981 and 2014) where the E-

W strike of the fault turns into NW. This change in strike is in accordance with the compressional stress regime obtained from site 7. As for site 6, it is inspected along a pressure ridge formed along a branch of the main fault. In that area, the fault branch locally accommodates the contractional deformation induced by left-lateral faulting along the main fault trend. In other words, this compressional stress regime expresses the local variation in regional stress at structural complexities along the fault. Besides these local changes, the paleostress state deduced from the oldest generation of fault slip data measured in Pliocene and older rock units is characterized by a N135±15°E trending mean σ_1, with a transpressional stress regime. During the prevalence of this stress field, the E-W Dasht-e Bayaz fault was an oblique reverse dextral fault.

In the kinematic analysis, an important issue is the possibility of structural rotations due to progressive deformation. Evaluating such a possibility, we have used arrays of dikes intruded in the folded strata of the area (section 4; Fig. 4). Aside for the amazing similarity in trends of the oldest generation of dikes (N330±10°E) and the paleo-σ_1 we have obtained (σ_{hmax} = N315±15°E), the overall orientation of the dikes does not significantly vary along and across the strike of both the Mahyar and Dasht-e Bayaz faults (Fig. 4). The same orientations of the first set of dikes close to, and beyond the main fault traces indicates insignificant structural rotations due to the post injection strike-slip faulting. Therefore, in the absence of signs of gradual changes in geological markers like post Eocene dikes (see Figure 4), our results indicate a drastic change in the regional state of stress and in other words, a kinematic switch from dextral to sinistral faulting along the Dasht-e Bayaz fault during the Pliocene-Quaternary time. Currently, the Dasht-e Bayaz main fault zone, reactivated on 31 August 1968, contains several roughly E-W fault strands characterized by a coseismic sinistral mechanism superimposing the older reverse dextral kinematics of the main fault (Figs 8, 11 and 12).

6.2. Late Cenozoic stress fields in the Iranian Plateau, Alborz and Kopeh Dagh mountains

One of the most interesting issues concerning the accommodation of Arabia-Eurasian convergence in the Iranian plateau is the history of the evolution of stress regimes during Pliocene and Quaternary. Thanks to modern techniques, such as the inversion of focal mechanisms of earthquakes, our knowledge about the present-day state of stress has progressed. Whereas, there is still some ambiguity left concerning the interpretation of long-term changes in stress regime and the transition between successive stress regimes.

Temporal changes in the stress field of the Alborz range, Kopeh Dagh Mountains and north of the Lut block, as well as northwest Iran have been reported by several authors (e.g., Tchalenko et al., 1974; Abbassi and Shabanian, 1999; Jackson et al., 2002; Allen et al., 2003; Guest et al., 2006; Zanchi et al., 2006; Yassaghi and Madanipour, 2008; Abbassi and Farbod, 2009; Landgraf et al., 2009; Shabanian et al., 2010, 2012a; Farbod et al., 2011; Javidfakhr et al., 2011; Tadayon et al., 2017; Aflaki et al., 2018a, 2018b). The rate and style of deformation in north and northeast Iran have significantly changed during the late Cenozoic (e.g., Ritz et al., 2006; Shabanian et al., 2009b, 2010). The systematic fault kinematics studies in these regions have shown that the late Cenozoic stress changes had been drastic (e.g., Shabanian et al., 2010; Javidfakhr et al., 2011)

As for temporal changes, Tchalenko et al. (1974), during tectonic studies in the Tehran region, have noticed the possible occurrence of a post-Pleistocene change in the orientation of maximum horizontal compression (σ_1) from NW to NE, based on the pattern of post Eocene dikes, the style of folding and faulting in the alluvial formations. In the same region, Abbassi and Shabanian (1999) have found three distinct states of stress and a clockwise rotation in the stress field through the inversion of fault slip data mostly measured in Pliocene-Quaternary alluviums. According to their research, the oldest stress field was characterized by a NW-trending σ_1 that has changed into a N-S and then, into a NE-directed maximum compression affecting late Pleistocene to Holocene alluviums. Another interesting research in west-central Alborz (Axen et al., 2001), has led to the attainment of the first chronological framework for

554 a major tectonic reorganization in the Alborz Mountains. They have reported a dextral transpressional
555 movement along main faults parallel with the range (between 56 Ma and 7 Ma) before onset (ca. 3.4 Ma)
556 of the modern sinistral faulting on these faults.

557 In the Kopeh Dagh and Binalud mountains, the inversion of fault slip data measured in 39 sites
558 revealed temporal clockwise changes in the state of stress since 3.6 Ma (Shabanian et al., 2010); those
559 include the horizontal σ_1 oriented N140±10°E, N180±10°E and N30±15°E for the paleo, intermediate and
560 modern states of stress, respectively. Similar drastic temporal changes were reported in NNE Iran,
561 including the eastern Alborz and western Kopeh Dagh mountains (Javidfakhr et al., 2011). The analysis
562 of fault slip data in 48 sites led Javidfakhr et al. (2011) to characterize the three homogenous stress fields
563 as the maximum horizontal stress σ_1 orientated N135±20°E (paleostress), N185±15°E (intermediate) and
564 N36±20°E (modern stress) in the transitional zone between the eastern Alborz and western Kopeh Dagh
565 mountains. Farther south, Farbod et al. (2011) showed that a Pliocene-Quaternary older state of stress,
566 with a σ_1 orientated N150±20°E, was changed into a modern maximum compression of N45±15°E,
567 responsible for the active sinistral kinematics along the Doruneh fault system.

568 Other study reveals the same pattern of change in the stress field of northwest Iran (the Mianeh-
569 Mahneshan basin; Aflaki et al., 2018a). The NW-trending fold axes in the Upper Red Formation, folded
570 at the end of Middle Miocene, have been overprinted by two younger generations of NE and NW trending
571 folds in a time interval between Pliocene to Quaternary. The inversion results of fault slip data in this
572 region affirm that a compressional paleostress regime (Pliocene-Quaternary), with a N138°E trending σ_1,
573 has affected the area before the dominance of the present-day NE-oriented compression.

574 The recent study in the Sistan belt of eastern Iran (Jentzer et al., 2017), however, obtained three
575 distinct deformation stages during late Cenozoic, including (1) an E-W (N087±5°E) direction of σ_1
576 probably in the Late Miocene, (2) a late Pliocene ENE-WSW (N059±8°E) direction of σ_1 and (3) a late
577 Pliocene to present-day maximum compression (N026±8°E). The same authors proposed that during the
578 last ~10–5 Ma, the direction of compression has rotated about 60° counterclockwise in Sistan. The
579 kinematics of this region, especially from the regional geologic and geodynamic points of view, is

580 debatable. However, there is no other similar study in the Sistan belt enabling a comparison and the
581 evaluation of the accuracy of their results.

582 In summary, even though several studies confirm the occurrence of drastic changes in the dynamics
583 and consequently, in the kinematics of the north, east and northeastern Iran, these results are
584 geographically sparse and need absolute age-based chronologies in order to drawing firm conclusions on
585 the time of dominance and the geodynamic causes of the change in the context of the Arabia – Eurasia
586 convergence.

587

588 **6.3. Integration of our results at the regional scale**

589 After presenting a brief history of the related studies on the evolution of Late Cenozoic stress state
590 in the north, east and northeast of Iran, here, we put our results in a regional tectonic context in order to
591 evaluate the consistency of the results with other similar studies in the north, northwest and west of the
592 Dasht-e Bayaz area.

593 The results of inversion on both geological and seismological fault slip data indicate the dominance
594 of an active strike-slip tectonic regime characterized by a N45±05°E trending σ_1 in the Dasht-e Bayaz
595 area. There is a good consistency between this stress regime and the modern state of stress with an
596 average compression of N045°E reported along the Doruneh fault (Farbod et al., 2011). Farther north,
597 Shabanian et al. (2010) reported a modern state of stress in the Kopeh Dagh and Allah Dagh-Binalud
598 mountains (Fig. 15) characterized by a mean regional ~N030°E trending σ_1 axis. According to the results
599 of Javidfakhr et al. (2011), this modern state of stress prevails on the eastern Alborz and western Kopeh
600 Dagh mountains (mean regional ~N036°E trending σ_1 axis). Interestingly, the results mentioned above
601 cover geological domains with different structural patterns, geological histories and active tectonics,
602 while except for some local perturbations due to structural complexities, the modern state of stress
603 remains homogenous throughout the region.

As for the intermediate stress regime in the Dasht-e Bayaz area, the related maximum horizontal compression obtained in two sites was oriented as ~N009°E. Despite the few number of these stress solutions, at a larger scale, our results are completely in accordance with other studies done in the northeast of Iran (N180±10°E - Shabanian et al., 2010; Javidfakhr et al., 2011). Although there is no report of intermediate state of stress by Farbod et al. (2011) along the Doruneh fault region, Tadayon et al. (2017) presented structural evidences for the prevalence of a penultimate N-S compression during the Plio-Quaternary time (see also Tadayon et al., 2018).

We have obtained a compressional stress regime characterized by a N135±15°E trending mean σ_1 as paleostress state, indicating that the currently left-lateral Dasht-e Bayaz fault had been reverse right-lateral during a certain period of time. As an example, the coseismic rupture of the 1968 earthquake cuts along the main fault trace at the northern border of the Chah Deraz pull-apart (Figs 3 and 6). In that area, S-shaped sigmoidal lenses within the fault core (Fig. 10d) indicate an older dextral component for the main fault. A similar paleostress state has been reported in the Kopeh Dagh and the transition zone between the Alborz and Kopeh Dagh mountains (N140±10°E trending σ1 - Shabanian et al., 2010; Javidfakhr et al., 2011). A close stress orientation (N150±20°E trending σ1) and structural configuration were also determined along the Doruneh fault (Farbod et al., 2011; see also Javadi et al., 2013, 2015; Tadayon et al., 2017 and 2018). It is worthy to note that farther west, along the Kuh-e Sarhangi and Kuh-e Faghan faults, Nozaem et al. (2013) and Calzolari et al. (2016 and 2018) have reported a NW-SE directed maximum compression which is responsible for dextral faulting along these faults during the Quaternary time and should not be compared to the paleostress σ_1 direction we are discussing here.

The general consistency between the results on the kinematic history of the east, northeast and north of the Arabia-Eurasia collision zone (Abbassi and Shabanian, 1999; Abbassi and Farbod, 2009; Shabanian et al., 2010, 2012b; Farbod et al., 2011; Javidfakhr et al., 2011; Javadi et al., 2013, 2015; Aflaki et al., 2017; Tadayon et al., 2017, 2018; this study) implies a homogenous transfer of stress during different periods of time, regardless of the geodynamic boundaries. Our results confirm that the Zagros collision zone, and its hinterland domain were mechanically coupled during, at least, late Miocene-

Quaternary times (e.g., Tadayon et al., 2018). Such kinds of systematic regional change in the late Miocene to present-day states of stress and kinematics of crustal-scale faults discard the possibility of systematic block rotations around vertical axes in the region between Dasht-e-Bayaz, Doruneh and Kopeh Dagh.

Despite the coherency between our results and those obtained in the northern regions, the history of stress changes along the Dasht-e Bayaz fault differs from what is recently obtained along the Sistan Suture zone (Jentzer et al., 2017). Jentzer et al. (2017) presented different sets of fault slip data related to three successive stress states indicating an anticlockwise rotation in the direction of maximum compression from a Late Miocene E-W directed σ1 to a late Pliocene to present-day maximum compression directed N026±8°E (see the section 6.2 for more details). Their anticlockwise rotation pattern is contrary to the history we found around the Dasht-e Bayaz and Abiz faults.

As for the age, there is no general consensus on the timing of the aforesaid changes in the stress state; for example, according to the morphotectonic analysis along the Mosha and Taleghan faults in Alborz, Ritz et al. (2006) suggested that the change from a N-S compression (compressional tectonic regime) to the present-day NNE-trending compression should have occurred between 1 and 1.5 Ma. Shabanian et al. (2012a) showed geological evidence for late Cenozoic volcanism (dikes and volcanic domes) coeval with the prevalence of the paleostress state (a NW trending maximum compression) in the transition zone between the Kopeh Dagh and Binalud mountains. The last phase of volcanism was dated at 2.4 Ma (Ar-Ar dating of dacitic volcanic domes) and subsequently, a volcanic dome has been right-laterally displaced by the N-S Chakaneh Fault, reactivated in the modern stress state (Shabanian et al., 2009b, 2012a). Accordingly, they proposed a maximum age of 2.4 Ma (close to the border of Pliocene and Quaternary) for the end of the paleostress prevalence. In the Mahneshan area (NW Iran; Fig. 15), Aflaki et al. (2018a) proposed that the last drastic change in the stress regime into the present-day stress state (a NE trending maximum compression) has taken place at the Pliocene-Quaternary boundary. Around the Doruneh fault (north of the Lut Block), however, Tadayon et al. (2018) suggested that the switch from an early NW-oriented σ_1 to the penultimate N-S maximum compression has occurred at the

Miocene-Pliocene boundary (5-6 Ma) and this change has been the source of an important cooling/exhumation in the area.

Nowadays, a drastic change in the Plio-Quaternary tectonic regime throughout the Iranian plateau and the surrounding deformation domains is a geological fact, thanks to different researches carried out during the last two decades (e.g., Abbassi and Shabanian, 1999; Regard et al., 2005; Shabanian et al., 2010, 2012a; Javidfakhr et al., 2011; Farbod et al., 2011; Tadayon et al., 2017; Jentzer et al., 2017; Aflaki et al., 2018a). The regional extent of these similar changes in distant Pliocene-Quaternary stress fields clearly discards the possibility of block/stress rotation during progressive deformation. However, the possible causes of change in stress regime, especially in E and N of Iran, remains unclear. This change may be due to the onset of the northward subduction of the South Caspian Basin, and/or changes in the structural configuration or in the lithospheric characteristics of N and NE Iran during an evolving collisional convergence (Shabanian et al., 2012a). In other words, it may correspond to a major regional reorganization of the plate boundary, following the transition from an infant to a mature stage of continental collision (Tadayon et al., 2018).

6.4. Tectonic scenario and kinematic model

According to the model frequently applied in the east and northeast of Iran, originally proposed by Jackson and McKenzie, (1984), an uneven distribution of N-S right-lateral shear between Central Iran and Afghanistan and its westward decrease caused a clockwise rotation of fault bounded blocks north of ~34°N (Walker et al., 2004; Walker and Jackson, 2004). The model tends to explain the structural features of the northern Lut block by the concept of clockwise rotation around vertical axes (for the basic assumptions of the model see Farbod et al., 2011). This block rotation model was questioned about its lack of ability in explaining the prominent curvature and the other complexities along the Doruneh Fault System (see Farbod et al., 2011 for detail). For example, Farbod et al. (2011), showed that to attain the present-day geometry of the DFS, the fault trace needs to rotate clockwise in the eastern part and

counterclockwise in the western part. It is noteworthy that structural deflections and internal deformation, due to local dragging or compression caused by faults or thrust zones, have usually been interpreted as systematic block rotations around vertical axes (e.g., Walker et al., 2004).

The occurrence of pre-Pliocene dextral faulting on E-W trends distributed across Central Iran (Javadi et al., 2013, 2015; Nozaem et al., 2013; Bagheri et al., 2016; Calzolari et al., 2016, 2018; Tadayon et al., 2017) and the Quaternary kinematic shifts along the Doruneh and Dasht-e Bayaz faults (Farbod et al., 2011; Javadi et al., 2015; this study), which clearly indicate a homogenous regional stress field distribution and coeval evolution of the intracontinental deformation in Central Iran, are not coherent with the block rotation model (see Tadayon et al., 2018 for discussion). The paleomagnetic data of Mattei et al. (2012) also do not show any systematic clockwise rotation over the Neogene in the region. The most recent study by Mattei et al. (2019) provides new paleomagnetic data on the Kopeh Dagh. They report that paleomagnetic rotations (the mean of 11.3±9.4° clockwise rotation) occurred in the Kopeh Dagh belt between ~6–4 Ma and ≈2 Ma, before the onset of the westward extrusion of the South Caspian Block. In their studies, Mattei et al. (2017 and 2019) also emphasize that their oroclinal model does not correspond to the present-day kinematics of the studied areas (Alborz and Kopeh Dagh) and the rotation was stopped before the onset of the present-day kinematics at ~2 Ma.

In our tectonic scenario (Figs 16 and 17), right-lateral shear is considered as the main mechanism for the accommodation of the Arabia-Eurasia convergence, but it is not necessarily the case everywhere in E and NE Iran. As for the Lut block, the GPS velocity vectors show a northward (N013°E) block motion with respect to Eurasia (Walpersdorf et al., 2014). In the north of latitude of 34°N (corresponding to the E-trending Dasht-e Bayaz fault), the N-S right-lateral shear interrupts and does not continue to the north. Beyond this latitude, the convergence is mainly accommodated by crustal shortening across NW-trending reverse/thrust faults. The Ferdows reverse fault zone, the Jangal and Khaf thrust faults and the eastern reverse termination of the Doruneh fault (Farbod et al., 2011) as well as the restraining fault terminations in the southern flank of Binalud (Shabanian et al., 2012b) and the Fariman area (Aflaki et al., 2019) are

among the most important NW-striking reverse faults confirming our tectonic scenario in northeastern Iran.

To the north and approximately at the latitude 36°N, the right-lateral shear gradually appears along the NE boundary of the Arabia – Eurasia collision zone and involves the NNW-trending faults (instead of the N-S dextral faults to the south) going through the Kopeh Dagh Mountains. The distance between these two fault systems is occupied by a soft-linking restraining relay zone (Binalud-Fariman-Torbat-e Jam; Aflaki et al., 2019) in which the mechanism of faulting is preferably reverse to revers dextral, while farther north in the Kopeh Dagh, it is pure dextral strike-slip. In other words, the N-S right-lateral shear between Iran and Afghanistan that had been interrupted in the latitude 34° N (corresponding to the Dasht-e Bayaz fault) is recuperated gradually around the latitude of ~36°N, but this time along the NW-trending faults and against the Turan platform instead of the Helmand block (Afghanistan).

The integrated geological, seismological and InSAR investigations done by Aflaki et al. (2019), in the area affected by the 5th April 2017 Sefid Sang earthquake (Mw 6), showed that the dextral shear along the NNW-striking faults (i.e., Bakharden-Quchan and Hezar Masjed fault systems) is transferred southeast into WNW-striking transpressional terminations in the region between the Binalud Mountains and Doruneh fault (Fig. 17). The CMT and the first polarity solutions of the main shock and the two aftershocks of this seismic event, which occurred close to the southern termination of the Hezar Masjed fault system near the town of Fariman (Fig. 15), indicate a mainly reverse mechanism with a small dextral component (See Aflaki et al., 2019 for details). This event clearly reveals the dominance of reverse faulting in the southeastern end of Kopeh Dagh and the eastern termination of the Doruneh fault.

In summary, we suggest that the outstanding changes in the structural pattern of these regions are the cause of a significant change in the accommodation mechanism of convergence. It means major fault zones in the E and NE Iranian regions guide and control lithospheric block motions and their related velocity fields. In the offset and/or overlapping areas of these major fault zones the convergence is accommodated by internal deformation and shortening through reverse/thrust faulting and active folding

(e.g., Farbod et al., 2011; Aflaki et al., 2019). For instance, the pure strike-slip Doruneh fault becomes a typical reverse fault at its eastern end parallel to the other NW-trending reverse faults such as Ferdows, Khaf and Jangal. In this context the role of E-W sinistral faults such as the Doruneh, Dasht-e Bayaz and Niazabad faults can be explained through their setting in the regional structural pattern.

The Khaf and Jangal thrusts have been considered as probable sources for the Zuzan historical destructive earthquakes (Berberian, 2014) of 19 and 21 October of 1336 A.D., respectively. The 1 and 4 September 1968 Ferdows earthquakes (M_W 6.8 and M_W 5.5) also indicate significant tectonic activity of these reverse fault zone. The study of magnetic foliation vertical and oblique to the bedding of post Miocene folds in the Ferdows fault zone (Rashid et al., 2015) suggests that a cleavage system, not visible at the outcrop scale, has been developed as a consequence of recent shortening related to the activity of this thrust zone. All these observations reveal that, in the northern Lut, the NW-trending reverse/thrust fault zones accommodates substantial portion of the active deformation perpendicular to their strikes. The E-W strike-slip faults such as the Dasht-e Bayaz and Niazabad faults therefore retain their complementary role in the crustal shortening between these thrust zones (Fig. 2). It is worth mentioning that our kinematic model generally describes the northeastern border of Arabia-Eurasia collision zone and clearly it does not include the distant regions such as the eastern Alborz and internal blocks of Central Iran.

Summarizing all these observations on both the structural configuration and the present-day relative velocity field (Eurasia fixed) in east-northeast Iran, the Doruneh fault is a major boundary separating two distinct northern and southern domains (Fig. 16). Angular relationships between N-S dextral and E-W sinistral faults obviously change in these tectonic domains such that the northern domain is characterized by NNW-striking dextral and ENE-striking sinistral faults (e.g., Tchalenko and Berberian, 1975; Shabanian et al., 2009a, 2010; Javidfakhr et al., 2011), while, N-S dextral, E-W sinistral and NW-SE reverse/thrust faults are dominant in the southern domain. These different structural patterns lead to (1) the NNW extrusion of both Central Iran and western Kopeh Dagh towards the South Caspian Basin (Hollingsworth et al., 2006; Shabanian et al., 2009b) and (2) block translation and internal deformation

through crosswise strike-slip faulting accompanied by reverse/thrust faulting in confining wedge in the north and south of the Doruneh fault, respectively.

The details of these different processes are shown in Figure 17. The process of wedge confining at the edges of north-going blocks (Fig. 17a; due to a NE-trending compression) allows accommodating the internal deformation not absorbed by the lithospheric scale northwards motion of Central Iran relative to Eurasia. The block adjustment requiring for the accommodation of this internal deformation is done through crosswise faulting along N-S dextral and E-W sinistral faults (Fig. 17b-d). The active crosswise pattern of the faults and the almost symmetrical deformation in the four quadrants around their intersection zones (Figs 4 and 17) indicate the same structural significance for the N-S and E-W faults. However, the simultaneous activity of these crosswise fault sets is mechanically impossible; therefore, the fault sets must be operating in sequence (e.g., Freund, 1974). The sequence of recent seismic activities, producing sinistral faulting along both the western and eastern segments of the Dasht-e Bayaz fault and right-lateral faulting in the south of this system, could confirm this interaction (see Berberian et al., 1999; Walker et al., 2011). This active crosswise faulting also leads to the development of contractional (reverse/thrust) fault zones perpendicular to the overall direction of Arabia – Eurasia convergence accommodating two northward and eastward components of the convergence (Fig. 17).

We emphasize that this tectonic scenario is based on different geological and seismological observations (this study and the references cited above) on the eastern and northeastern boundaries of the Arabia – Eurasia convergence zone. We do not apply this scenario to kinematic complexities reported in other places in Central Iran. For example, dextral faulting along the Kuh-e Sarhangi and Kuh-e Faghan faults in the northwest margin of the Lut block (Nozaem et al., 2013; Calzolari et al., 2016 and 2018) has been explained as a consequence of an excess dextral shear generated in the intrafault block bordered by the Doruneh fault to the north and the Dasht-e–Bayaz fault to the south. In this context, the Ferdows reverse fault zone partly accommodates internal deformation of the intrafault block (Nozaem et al., 2013). At first glance to our tectonic scenario, one may make a similar conclusion by assuming a component of

781 westward extrusion for the northern block of the Dasht-e Bayaz fault. However, deducing such the
782 conclusion needs detailed information on the difference of slip rates on the Doruneh and Dasht-e Bayaz
783 faults as well as the contribution of the Ferdows reverse fault zone in the accommodation of this
784 differential slip rate.

785 **7. Conclusion**

786 Our inversion analysis of fault kinematics data revealed signatures of three distinct stress fields in
787 the Dasht-e Bayaz area during Plio-Quaternary. Before the onset of the active left-lateral faulting along
788 the Dasht-e Bayaz fault, an old stress state characterized by a N135±15°E trending σ_1 was responsible for
789 the dextral transpressional movements. The consistency between the inversion results of both modern
790 geological fault slip data and the earthquake focal mechanisms reveals: (1) the absence of remarkable
791 change in the modern state of stress during the late Quaternary time, (2) the prevalence of a homogeneous
792 stress field in the brittle crust (above the ~17 km depth of seismogenic layer) of the Dasht-e Bayaz region
793 and (3) the lack of long-term stress perturbation due to the activity of the Dasht-e Bayaz fault.

794 Our observations indicate that the kinematic changes during the Pliocene – Quaternary times have
795 not been restricted to the northeastern part of the Iranian plateau. The general consistency between the
796 results on the kinematic history of the east, northeast and north of the Arabia – Eurasia collision zone
797 implies that a homogenous transfer of stress during, at least, late Miocene – Quaternary times, has taken
798 place due to the mechanical coupling of the Zagros collision and its hinterland domains.

799 We suggest that the region between Lut and Kopeh Dagh is divided by the Doruneh fault into two
800 northern and southern distinct tectonic domains. The northern domain is characterized by the extrusion of
801 fault-bounded blocks towards the north-northwest, while in the southern domain, the northward motion of
802 the central Iranian blocks occurs through structural and kinematic interactions between N-S dextral, E-W
803 sinistral and NW-striking reverse/thrust faults at the block boundaries without a need for symmetric block
804 rotations around vertical axes.

Acknowledgements

We would like to thank to Mr. Koreie and Mr. Fotovati from Geological Survey of Iran for their support and logistic assistance. We are grateful to municipality of Khezri-Dasht-e Bayaz and Sangan Iron Ore Complex for their support during field trips. We thank Mr. Lhôte and the staff of French Embassy in Tehran. We appreciate to A. Ghods and F. Sobouti in Institute for Advanced Studies in Basic Sciences in Zanjan. Very careful and insightful reviews by Federico Rossetti and two anonymous reviewers have greatly improved the manuscript. We are indebted to Editor Ling Chen for handling the manuscript.

References

Abbassi M.R., and E. Shabanian (1999), Evolution of the stress field in the Tehran region during the Quaternary, Third International Conference on Seismology and Earthquake Engineering, Tehran-Iran.

Abbassi, M.R., and Y. Farbod (2009), Faulting and folding in quaternary deposits of Tehran's piedmont (Iran), Journal of Asian Earth Sciences, 34, 522-531, doi:10.1016/j.jseaes.2008.08.001.

Aflaki, M., Shabanian, E., and Z. Davoodi (2017), Quaternary state of stress in the Mahneshan-Mianeh sedimentary basin, NW Iran, Scientific quarterly of Geoscience, Text in Persian with English abstract, 26, 102,

Aflaki, M., Shabanian, E., and Z. Davoodi (2018a), Signatures of Deformation Related to the Plio-Quaternary State of Stress in the Mahneshan-Mianeh Basin (NW Iran), Iranian J. of Seismology and Earthquake Engineering, Text in Persian with English abstract, 4th year, 4, 29-42.

Aflaki, M., Ghods, A., Mousavi, Z. , Shabanian, E., Vajedian, S., and M. Akbarzadeh (2018b), Seismotectonic characteristics of the 2017 Sefid Sang (Mw 6) earthquake, The 18th Iranian Geophysical Conference, 1-4.

828 Aflaki, M., Mousavi, Z., Ghods, A., Shabanian, E., Vajedian, S., and M. Akbarzadeh (2019), The 2017
829 Mw 6 Sefid Sang earthquake and its implication for the geodynamics of NE Iran, Geophysical
830 Journal International, 218(2), 1227-1245, DOI: 10.1093/gji/ggz172/5462654.

831 Alavi Naini, M., and A. Behruzi (1983), Geological quadrangle map of Iran, Map K-6, Gonabad sheet,
832 scale 1:250,000, Geological Survey of Iran, Tehran.

833 Allen, M.B., Ghassemi, M.R., Shahrabi, M., and M. Qorashi (2003), Accommodation of late Cenozoic
834 oblique shortening in the Alborz range, northern Iran, J. Struct. Geol., 25, 659-672.

835 Allmendinger, R.W., Strecker, M., Eremchuk, J.E., and P. Francis (1989), Neotectonic deformation of the
836 southern Puna plateau, NW Argentina, J. S. Am. Earth Sci., 2, 111-130.

837 Allmendinger, R.W., Cardozo, N., and D., Fisher (2013), Structural geology algorithms: Vectors and
838 tensors in structural geology, Cambridge University Press.

839 Ambraseys, N.N., and J.S. Tchalenko (1969), The Dasht-e-Bayaz (Iran) earthquake of August 31, 1968:
840 A field report, Bull. Seism. Soc. Am., 59, 1751-1792.

841 Ambraseys, N.N., and C.P. Melville (1982), A history of Persian earthquakes, Cambridge University
842 Press, Cambridge.

843 Angelier, J., (1979), Determination of mean principal stresses for a given fault population,
844 Tectonophysics, 56, T17-T26.

845 Angelier, J., (1984), Tectonic analysis of fault slip data sets, J. Geophys. Res., 89, 5835-5848.

846 Angelier, J., (1990), Inversion of field data in fault tectonics to obtain the regional stress. III-a new rapid
847 direct inversion method by analytical means, Geophys. J. Int., 103, 363-376.

848 Authemayou, C., Chardon, D., Bellier, O., Malekzade, Z., Shabanian, E., and M. Abbassi (2006), Late
849 Cenozoic partitioning of oblique plate convergence in the Zagros fold-and thrust belt (Iran),
850 Tectonics, 25, TC3002, doi:10.1029/2005TCOO1860.

851 Authemayou, C., Bellier, O., Chardon, D., Benedetti, L., Malekzade, Z., Claude, C.,
852 Angeletti, B., Shabanian, E., and M.R. Abbassi (2009), Quaternary slip-rates of the
853 Kazerun and the Main Recent Faults: active strike-slip partitioning in the Zagros fold and-thrust belt,
854 Geophys. J. Int., 178, 524-540, doi:10.1111/j.1365-246X.2009.04191.x.

855 Axen G.J., Lam, P.S., Grove, M., Stockli, D.F., and J. Hassanzadeh (2001), Exhumation of the west-
856 central Alborz Mountains, Iran, Caspian subsidence, and collision-related tectonics, Geology, 29,
857 559-562.

858 Bagheri, S., Madhanifard, R., and F. Zahabi (2016), Kinematics of the Great Kavir fault inferred from a
859 structural analysis of the Pees Kuh Complex, Jandaq area, central Iran, Geological Society of
860 America Special Papers, 525, doi:10.1130/2016.2525.

861 Bellier, O., and M.L. Zoback (1995), Recent state of stress change in the Walker Lane zone, western
862 Basin and Range province, United States, Tectonics, 14, 564-593, doi:10.1029/94TC00596.

863 Berberian, M., (1981), Active faulting and tectonics of Iran, In: Gupta H.K., and F.M. Delany (Editors)
864 Zagros, Hindu Kush, Himalaya Geodynamic Evolution, Am. Geophys. Union, Geodyn. S. 3, 33-69,
865 doi:10.1029/GD003.

866 Berberian, M., (1995), Natural Hazards and the First Earthquake Catalogue of Iran, Volume 1: Historical
867 Hazards in Iran Prior to 1900, Int. Inst. Earthq. Eng. & Seismology, Tehran, Iran.

868 Berberian, M., Jackson, J.A., Qorashi, M., Khatib, M.M., Priestley, K., Talebian, M., and M. Ghafuri-
869 Ashtiani (1999), The 1997 May 10 Zirkuh (Qa'enat) earthquake (Mw 7.2): faulting along the Sistan
870 suture zone of eastern Iran, Geophys. J. Int., 136, 671-94, doi:10.1046/j.1365-246x.1999.00762.x.

871 Berberian, M., (2014), Earthquakes and Coseismic Surface Faulting on the Iranian Plateau, Elsevier,
872 Developments in Earth Surface Processes, 17, 2-714.

873 Bott, M.H.P., (1959), The mechanics of oblique slip faulting, Geol. Mag. 96, 109-117.

874 Braud, J., and L.E. Ricou (1975), Eléments de continuité entre le Zagros et la Turquie du Sud-Est,
875 Bulletin de la Société Géologique de France, 17, 1015-23.

876 Burg, J.-P., (2018), Geology of the onshore Makran accretionary wedge: Synthesis and tectonic
877 interpretation, Earth-Science Reviews, 185, 1210-1231, doi:10.1016/j.earscirev.2018.09.011.

878 Calzolari, G., Rossetti, F., Della Seta, M., Nozaem, R., Olivetti, V., Balestrieri, M.L., Cosentino, D.,
879 Faccenna, C., Stuart, F.M., and G. Vignaroli, (2015), Spatio-temporal evolution of intraplate strike-
880 slip faulting: The Neogene–Quaternary Kuh-e-Faghan Fault, central Iran, Geol. Soc. Am. Bull., 128,
881 374-396, doi:10.1130/B31266.1.

882 Calzolari, G., Della Seta, M., Rossetti, F., Nozaem, R., Vignaroli, G., Cosentino, D., and C. Faccenna
883 (2016), Geomorphic signal of active faulting at the northern edge of Lut Block: Insights on the
884 kinematic scenario of Central Iran, Tectonics, 35, 76-102, doi:10.1002/ 2015TC003869.

885 Calzolari, G., Rossetti, F., Ault, Alexis K., Lucci, F., Olivetti, V., and R. Nozaem (2018), Hematite (U-
886 Th)/He thermochronometry constrains intraplate strike-slip faulting on the Kuh-e-Faghan Fault,
887 central Iran, Tectonophysics, 728-729, 41-54, doi:10.1016/j.tecto.2018.01.023.

888 Carey, E., and B. Brunier (1974), Analyse théorique et numérique un modèle mécanique élémentaire
889 appliqué à l'étude d'une population de failles, C. R. Acad. Sci., 279, 891-894.

890 Carey, E. (1979), Recherche des directions principales contraintes associées au jeu d'une population de
891 failles, Rev. Geol. Dyn. Geogr. Phys., 21, 57 - 66.

892 Carey-Gailhardis, E., and J.L. Mercier (1987), A numerical method for determining the state of stress
893 using focal mechanisms of earthquake populations: application to Tibetan teleseisms and
894 microseismicity of Southern Peru, Earth Planet. Sci. Lett., 82, 165-179.

895 Carey-Gailhardis, E., and J.L. Mercier (1992), Regional state of stress, fault kinematics and adjustments
896 of blocks in a fractured body of rocks: application to the microseismicity of the Rhine graben, J.
897 Struct. Geol., 14, 1007-1017.

898 Cisternas, A., and H. Philip (1997), Seismotectonics of the Mediterranean region and the Caucasus,
899 In: Giardini, D., and S. Balassanian (Editors), Historical and Prehistorical Earthquakes in the
900 Caucasus, Kluwer Academic Publishing, Dordrecht, Netherlands, 39-77.

901 Dooley T.P., and G. Schreurs (2012), Analogue modelling of intraplate strike-slip tectonics: A review and
902 new experimental results, Tectonophysics, 574-575, 1-71.

903 Etchecopar, A., (1984), Etude des états de contraintes en tectonique cassante et simulation de
904 deformations plastiques (approche mathématique), thèse d'Etat, Université Montpellier II, France.

905 Farbod, Y., Bellier, O., Shabanian, E., and M.R. Abbassi (2011), Geomorphic and structural variations
906 along the Doruneh Fault System (Central Iran), Tectonics, 30, TC6014, doi:10.1029/2011TC002889.

907 Farbod, Y., Shabanian, E., Bellier, O., Abbassi, M. R., Braucher, R., Benedetti, L., Bourles, D., and K.
908 Hessami (2016), Spatial variations in late Quaternary slip rates along the Doruneh fault system
909 (central Iran), Tectonics, 35, 386-406.

910 Fauvelet, E., and J. Eftekhar-Nezhad (1991), Geological quadrangle map of Iran, Map K-7, Qayen sheet,
911 scale 1:250,000, Geological Survey of Iran, Tehran.

912 Foroutan, M., Meyer, B., Sébrier, M., Nazari, H., Murray, A.S., Le Dortz, K., Shokri, M.A., Arnold, M.,
913 Aumaître, G., Bourlès, D., Keddadouche, K., Solaymani-Azad, S., and M.J. Bolourchi (2014), Late

914 Pleistocene-Holocene right slip rate and paleoseismology of the Nayband fault, western margin of
915 the Lut block, Iran, J. Geophys. Res., 119, 3517-3560, doi:10.1002/2013JB010746.

916 Freund, R., (1974), Kinematics of transform and transcurrent faults, Tectonophysics, 21, 93-134.

917 Fry, N., (1999), Striated faults: visual appreciation of their constraint on possible paleostress tensors, J.
918 Struct. Geol., 21, 7-21.

919 Ghods, A., Shabanian, E., Bergman, E., Faridi, M., Donner, S., Mortezanejad, G., and A. Aziz-Zanjani,
920 (2015), The Varzaghan–Ahar, Iran, Earthquake Doublet (Mw 6.4, 6.2): implications for the
921 geodynamics of northwest Iran, Geophys. J. Int., 203, 522-540, doi:10.1093/gji/ggv306.

922 Guest, B., Stockli, D.F., Grove, M., Axen, G.J., Lam, P.S., and J. Hassanzadeh (2006), Thermal
923 histories from the central Alborz mountains, northern Iran: implications for the spatial and temporal
924 distribution of deformation in northern Iran, Geol. Soc. Am. Bull., 118, 1507-1521.

925 Haghipour, A., and M. Amidi (1980), The November 14 to December 25, 1979, Ghaenat earthquakes of
926 northeast Iran and their tectonic implications, Bull. Seism. Soc. Am., 70, 1751-1757.

927 Heidbach, O., Rajabi, M., Reiter, K., Ziegler, M., and WSM Team (2016), World Stress Map Database
928 Release, GFZ Data Services, doi:10.5880/WSM.2016.001.

929 Hessami, K., Jamali, F., and H. Tabassi (2003), Major active faults of Iran, scale 1:2,500,000,
930 International Institute of Earthquake Engineering and Seismology, Iran-Tehran.

931 Hippolyte, J.-C., Angelier, J., Nury, D., Bergerat, F., and G. Guieu (1993), Tectonic-stratigraphic record
932 of paleostress time changes in the Oligocene basins of the Provence, southern France,
933 Tectonophysics, 226, 15-35.

Hippolyte, J.-C., Bergerat, F., Gordon, M.B., Bellier, O., and N. Espurt (2012), Keys and pitfalls in mesoscale fault analysis and paleostress reconstructions, the use of Angelier's methods, Tectonophysics, 581, 144-162, doi:10.1016/j.tecto.2012.01.012.

Hollingsworth, J., Jackson, J., Walker, R.T., Gheitanchi, M.R., and M.J. Bolourchi (2006), Strike-slip faulting, rotation and along-strike elongation in the Kopeh Dagh Mountains, NE Iran, Geophys. J. Int., 166, 1161-1177, doi:10.1111/j.1365-246X.2006.02983.x.

Jackson, J., and D. McKenzie (1984), Active tectonics of the Alpine-Himalayan belt between Turkey and Pakistan, Geophys. J. R. astr. Soc., 77, 185-264.

Jackson, J., Priestley, K., Allen, M., and M. Berberian (2002), Active tectonics of the South Caspian Basin, Geophys. J. Int., 148, 214-245.

Javadi, H.R., Ghassemi, M.R., Shahpasandzadeh, M., Guest, B., Esterabi-Ashtiani, M., Yassaghi, A., and M. Kouhpeyma (2013), History of faulting on the Doruneh Fault System: Implications for the kinematic changes of the Central Iranian Microplate, Geol. Mag., 150, 651-672, doi:10.1017/s0016756812000751.

Javadi, H.R., Esterabi-Ashtiani, M., Guest, B., Yassaghi, A., Ghassemi, M.R., Shahpasandzadeh, M., and A. Naeimi (2015), Tectonic reversal of the western Doruneh Fault System: Implications for Central Asian tectonics, Tectonics, 34, doi:10.1002/2015TC003931.

Javidfakhr, B., Bellier, O., Shabanian, E., Ahmadian, S., and A., Saidi (2011), Plio–Quaternary tectonic regime changes in the transition zone between Alborz and Kopeh Dagh mountain ranges (NE Iran), Tectonophysics, 506, 86-108, doi:10.1016/j.tecto.2011.04.013.

Jentzer, M., Fournier, M., Agard, P., Omrani, J., Khatib, M. M., and H. Whitechurch (2017), Neogene to Present paleostress field in Eastern Iran (Sistan belt) and implications for regional geodynamics, Tectonics, 36, 321-339, doi:10.1002/2016tc004275.

Karakhanian, A.S., Trifonov, V.G., Philip, H., Avagyan, A., Hessami, K., Jamali, F., Salih Bayraktutan, M., Bagdassarian, H., Arakelian, S., Davtian, V., and A. Adilkhanyan, (2004), Active faulting and natural hazards in Armenia, eastern Turkey and northwestern Iran, Tectonophysics, 380,189-219, doi:10.1016/j.tecto.2003.09.020.

Landgraf, A., Ballato, P., Strecker, M.R., Friedrich, A., Tabatabaei, S.H., and M. Shahpasandzadeh (2009), Fault-kinematic and geomorphic observations along the North Tehran Thrust and Mosha Fasham Fault, Alborz mountains Iran: implications for fault-system evolution and interaction in a changing tectonic regime, Geophys. J. Int. 177, 676-690, doi:10.1111/j.1365-246X.2009.04089.x.

Marrett, R. A., and R.W. Allmendinger (1990), Kinematic analysis of fault-slip data, J. Struct. Geol., 12, 973-986.

Mattei, M., Cifelli, F., Muttoni, G., Zanchi, A., Berra, F., Mossavvari, F., and S.A. Eshraghi (2012), Neogene block rotation in Central Iran: Evidence from paleomagnetic data, Geol. Soc. Am. Bull., 124, 943-956, doi:10.1130/B30479.1.

Mattei, M., Cifelli, F., Alimohammadian, H., Rashid, H., Winkler, A., Sagnotti, L. (2017), Oroclinal bending in the Alborz Mountains (northern Iran): new constraints on the age of South Caspian subduction and extrusion tectonics, Gondwana Research 42, 13–28. https://doi.org/10.1016/j.gr.2016.10.003.

Mattei, M., Visconti, A. L., Cifelli, F., Nozaem, R., Winkler, A. and Sagnotti L. (2019), Clockwise paleomagnetic rotations in northeastern Iran: Major implications on recent geodynamic evolution of outer sectors of the Arabia-Eurasia collision zone, Gondwana Research 71, 194–209, https://doi.org/10.1016/j.gr.2019.01.018.

978 Mercier, J.L., Carey-Gailhardis, E., and M. Sébrier (1991), Paleostress determinations from fault
979 kinematics: application to the neotectonics of the Himalayan-Tibet and the central Andes, Philos.
980 Trans. R. Soc., 337, 41-52.

981 Meyer, B., and K. Le Dortz (2007), Strike-slip kinematics in Central and Eastern Iran: estimating fault
982 slip-rates averaged over the Holocene, Tectonics, 6, TC5009, doi:10.1029/2006TC002073, 2007.

983 Mohammadi Gharetapeh, A., Gholami, E., Khatib, M. M., Golchin, M. (2014), Development of structures
984 in a shear stress regime in East Dasht-e Bayaz Fault Zone (East of Iran), Journal of Tethys, 2(2),
985 101–111.

986 Molnar, P., and K.E. Dayem (2010), Major intracontinental strike-slip faults and contrasts in lithospheric
987 strength, Geosphere, 6, 444-467.

988 Momeni, S.M., and M. Tatar (2018), Mainshocks/aftershocks study of the August 2012 earthquake
989 doublet on Ahar-Varzaghan complex fault system (NW Iran), Phys. Earth Planet. Inter., 283, 67-81.

990 Mousavi, Z., Walpersdorf, A., Walker, R.T., Tavakoli, F., Pathier, E., Nankali, H., Nilfouroushan, F., and
991 Y. Djamour (2013), Global Positioning System constraints on the active tectonics of NE Iran and the
992 South Caspian region, Earth Planet. Sci. Lett., 377-378, 287-298, doi:10.1016/j.epsl.2013.07.007.

993 Nemcok, M., and R.J. Lisle (1995), A stress inversion procedure for polyphase fault slip data sets, J.
994 Struct. Geol., 17, 1445-1453.

995 Nozaem, R., Mohajjel, M., Rossetti, F., Della Seta, M., Vignaroli, G., Yassaghi, A., Salvini, F., and M.
996 Eliassi (2013), Post-Neogene right-lateral strike-slip tectonics at the north-western edge of the Lut
997 Block (Kuh-e–Sarhangi Fault), Central Iran, Tectonophysics, 589, 220-233,
998 doi:10.1016/j.tecto.2013.01.001.

999 Rashid, H., Cifelli, F., Mattei M. (2015), Late folding-related magnetic foliation in the active Ferdows
1000 (northeastern Iran) thrust–fold system, Journal of Asian Earth Sciences 108, 48–57,
1001 http://dx.doi.org/10.1016/j.jseaes.2015.04.023.

1002 Regard, V., Bellier, O., Thomas, J.-C., Bourlès, D., Bonnet, S., Abbassi, M.R., Braucher, R., Mercier, J.,
1003 Shabanian, E., Soleymani, S., and K. Feghhi (2005), Cumulative right-lateral fault slip rate across the
1004 Zagros-Makran transfer zone: role of the Minab-Zendan fault system in accommodating Arabia-
1005 Eurasia convergence in southeast Iran, Geophys. J. Int., 162, 177-203, doi:10.1111/j.1365-
1006 246X.2005.02558.x.

1007 Regard, V., Bellier, O., Braucher, R., Gasse, F., Bourlès, D., Mercier, J., Thomas, J.-C., Abbassi, M.R.,
1008 Shabanian, E., and S. Soleymani (2006), ^{10}Be dating of alluvial deposits from Southeastern Iran (the
1009 Hormoz Strait area), Palaeogeogr. Palaeoclimatol. Palaeoecol., 242, 36-53,
1010 doi:10.1016/j.palaeo.2006.05.012.

1011 Reilinger, R., McClusky, S., Vernant, P., Lawrence, S., Ergintav, S., Cakmak, R., Ozener, H., Kadirov,
1012 F., Guliev, I., Stepanyan, R., Nadariya, M., Hahubia, G., Mahmoud, S., Sakr, K., ArRajehi, A.,
1013 Paradissis, D., Al-Aydrus, A., Prilepin, M., Guseva, T., Evren, E., Dmitrotsa, A., Filikov, S.V.,
1014 Gomez, F., Al-Ghazzi, R., and G. Karam (2006), GPS constraints on continental deformation in the
1015 Africa-Arabia-Eurasia continental collision zone and implications for the dynamics of plate
1016 interactions, J. Geophys. Res. 111, B05411, doi:10.1029/2005JB004051.

1017 Ricou, L.E., Braud, J., and J.H. Bruhnn (1977), Le Zagros, Mem. H. Ser. Soc. Geol. Fr., 8, 33-52.

1018 Ritz, J.-F., and A. Taboada (1993), Revolution stress ellipsoids in brittle tectonics resulting from an
1019 uncritical use of inverse methods, Bull. Soc. Geol. Fr., 164, 519-531.

1020 Ritz, J.-F., Nazari, H., Ghassemi, A., Salamati, R., Shafei, A., Solaymani, S., and P.Vernant (2006),
1021 Active transtension inside Central Alborz: a new insight into northern Iran– southern Caspian
1022 geodynamics, Geology, 34, 477-480, doi:10.1130/ G22319.1.

1023 Rossetti, F., Storti, F., and A.L. Laufer (2002), Brittle architecture of the Lanterman Fault and its impact
1024 on the final terrane assembly in north Victoria Land, Antarctica, Journal of the Geological Society,
1025 159, 159-173.

1026 Salvini, F., and F. Storti (1999), Cenozoic tectonic lineaments of the Terra Nova Bay region, Ross
1027 Embayment, Antarctica, Global Planetary Change, 23, 129-144.

1028 Shabanian, E., Siame, L., Bellier, O., Benedetti, L., and M.R. Abbassi (2009a), Quaternary slip rates
1029 along the northeastern boundary of the Arabia–Eurasia collision zone (Kopeh Dagh Mountains,
1030 Northeast Iran), Geophys. J. Int., 178, 1055-1077, doi:10.1111/ j.1365-246X.2009.04183.x.

1031 Shabanian, E., Bellier, O., Siame, L., Arnaud, N., Abbassi, M.R., and J.-J. Cochemé (2009b), New
1032 tectonic configuration in NE Iran: active strike–slip faulting between the Kopeh Dagh and Binalud
1033 mountains, Tectonics, 28, TC5002, doi:10.1029/2008TC002444.

1034 Shabanian, E., Bellier, O., Abbassi, M.R., Siame, L., and Y. Farbod (2010), Plio-Quaternary stress states
1035 in NE Iran: Kopeh Dagh and Allah Dagh-Binalud mountain ranges, Tectonophysics, 480, 280-304,
1036 doi:10.1016/j.tecto.2009.10.022.

1037 Shabanian, E., Acocella, V., Gioncada, A., Ghasemi, H. and O. Bellier (2012a), Structural control on
1038 volcanism in intraplate post collisional settings: Late Cenozoic to Quaternary examples of Iran and
1039 Eastern Turkey, Tectonics, 31(3), TC3013.

1040 Shabanian, E., Bellier, O., Siame, L., Abbassi, M.R., Bourlès, D., Braucher, R., and Y. Farbod (2012b),
1041 The Binalud Mountains: A key piece for the geodynamic puzzle of NE Iran, Tectonics, 31, TC6003,
1042 doi:10.1029/2012TC003183.

1043 Shan, J., Suen, H., and G. Lin (2003), Separation of polyphase fault/slip data: an objective function
1044 algorithm based on hard division, J. Struct. Geol., 25, 829-840.

1045 Tadayon, M., Rossetti, F., Zattin, M., Nozaem, R., Calzolari, G., Madanipour, S., and F. Salvini (2017),
1046 The post-Eocene evolution of the Doruneh Fault region (Central Iran): The intraplate response to the
1047 reorganization of the Arabia-Eurasia collision zone, Tectonics, 36, 3038-3064.

1048 Tadayon, M., Rossetti, F., Zattin, M., Calzolari, G., Nozaem, R., Salvini, F., Faccenna, C., and P.
1049 Khodabakhshi (2018), The long-term evolution of the Doruneh Fault region (Central Iran): A key to
1050 understanding the spatio-temporal tectonic evolution in the hinterland of the Zagros convergence
1051 zone, Geological Journal, 1-26, doi:10.1002/gj.3241.

1052 Taghipour, K., Khatib, M.M., Heyhat, M.R., Shabanian, E., and A. Vaezihir (2018), Evidence for
1053 distributed active strike-slip faulting in NW Iran: The Maragheh and Salmas fault zones,
1054 Tectonophysics, 742, 15-33.

1055 Talebian, M., and J. Jackson (2004), A reappraisal of earthquake focal mechanisms and active
1056 shortening in the Zagros mountains of Iran, Geophys. J. Int., 156, 506-526.

1057 Tavakoli, F., Walpersdorf, A., Authemayou, C., Nankali, H.R., Hatzfeld, D., Tatar, M., Djamour, Y.,
1058 Nilforoushan, F., and N. Cotte (2008), Distribution of the right-lateral strike-slip motion from the
1059 Main Recent Fault to the Kazerun Fault System (Zagros, Iran): Evidence from present-day GPS
1060 velocities, Earth Planet. Sci. Lett, 275, 342–347, doi:10.1016/j.epsl.2008.08.030.

1061 Tchalenko, J.S., and N.N. Ambraseys (1970), Structural analysis of the Dasht-e Bayaz (Iran) earthquake
1062 fractures, Geol. Soc. Am. Bull., 81, 41-60.

1063 Tchalenko, J.S., Braud, J., and M. Berberian (1974), Discovery of three earthquake faults in Iran, Nature,
1064 248, 661-663.

1065 Tchalenko, J.S., and M. Berberian (1975), Dasht-e-Bayaz fault, Iran: earthquake and earlier related
1066 structures in bed-rock, Geol. Soc. Am. Bull., 86, 703-709.

1067 Tranos, M.D., (2015), TR method (TRM): a separation and stress inversion method for heterogeneous
1068 fault-slip data driven by Andersonian extensional and compressional stress regimes, J. Struct. Geol.,
1069 79, 57-74, doi:10.1016/j.jsg.2015.07.006.

1070 Tranos, M.D., (2018), The use of Stress Tensor Discriminator Faults in separating heterogeneous fault-
1071 slip data with best-fit stress inversion methods, J. Struct. Geol., 107, 153-162.

1072 Vernant, P., Nilforoushan, F., Hatzfeld, D., Abbassi, M.R., Vigny, C., Masson, F., Nankali,
1073 H., Martinod, J., Ashtiani, A., Bayer, R., Tavakoli, F., and J. Chery (2004), Present-day crustal
1074 deformation and plate kinematics in the Middle East constrained by GPS measurements in Iran and
1075 northern Oman, Geophys. J. Int., 157, 381-398.

1076 Walker, R.T., Jackson, J., and C. Baker (2003), Thrust faulting in eastern Iran: source parameters and
1077 surface deformation of the 1978 Tabas and 1968 Ferdows earthquake sequences, Geophys. J. Int.,
1078 152, 749-765.

1079 Walker, R.T., and J. Jackson (2004), Active tectonics and late Cenozoic strain distribution in central and
1080 eastern Iran, Tectonics, 23, TC5010, doi:10.1029/2003TC001529.

1081 Walker, R.T., Jackson J., and C. Baker (2004), Active faulting and seismicity of the Dasht-e-Bayaz
1082 region, eastern Iran, Geophys. J. Int., 157, 265-282.

1083 Walker, R.T., Bergman, E.A., Szeliga, W., and E.J. Fielding (2011), Insights into the 1968-1997 Dasht-e-
1084 Bayaz and Zirkuh earthquake sequences, eastern Iran, from calibrated relocations, InSAR and high-
1085 resolution satellite imagery, Geophys. J. Int., 187, 1577-1603, doi:10.1111/j.1365-
1086 246X.2011.05213.x.

Wallace R.E., (1951), Geometry of shearing stress and relation to faulting, J. Geol., 59, 118-130.

Walpersdorf, A., Hatzfeld, D., Nankali, H., Tavakoli, F., Nilforoushan, F., Tatar, M., Vernant, P., Chéry, J., and F. Masson (2006), Difference in the GPS deformation pattern of North and Central Zagros (Iran), Geophys. J. Int., 167, 1077-1088.

Walpersdorf, A., Manighetti, I., Mousavi, Z., Tavakoli, F., Vergnolle, M., Jadidi, A., Hatzfeld, D., Aghamohammadi, A., Bigot, A., Djamour, Y., Nankali, H., and M. Sedighi (2014), Present-day kinematics and fault slip rates in eastern Iran, derived from 11 years of GPS data, J. Geophys. Res., 119, 1359-1383.

Yassaghi, A., and S. Madanipour (2008), Influence of a transverse basement fault on along-strike variations in the geometry of an inverted normal fault: case study of the Mosha Fault, Central Alborz Range, Iran, J. Struct. Geol., 30, 1507–1519.

Zanchi, A., Berra, F., Mattei, M., Ghassemi, M.R., and J. Sabouri (2006), Inversion tectonics in central Alborz, Iran, J. Struct. Geol., 8, 2023-2037.

Zoback, M.L., (1989), State of stress and modern deformation of the basin and range province, J. Geophys. Res., 94, 7105-7128.

Figures

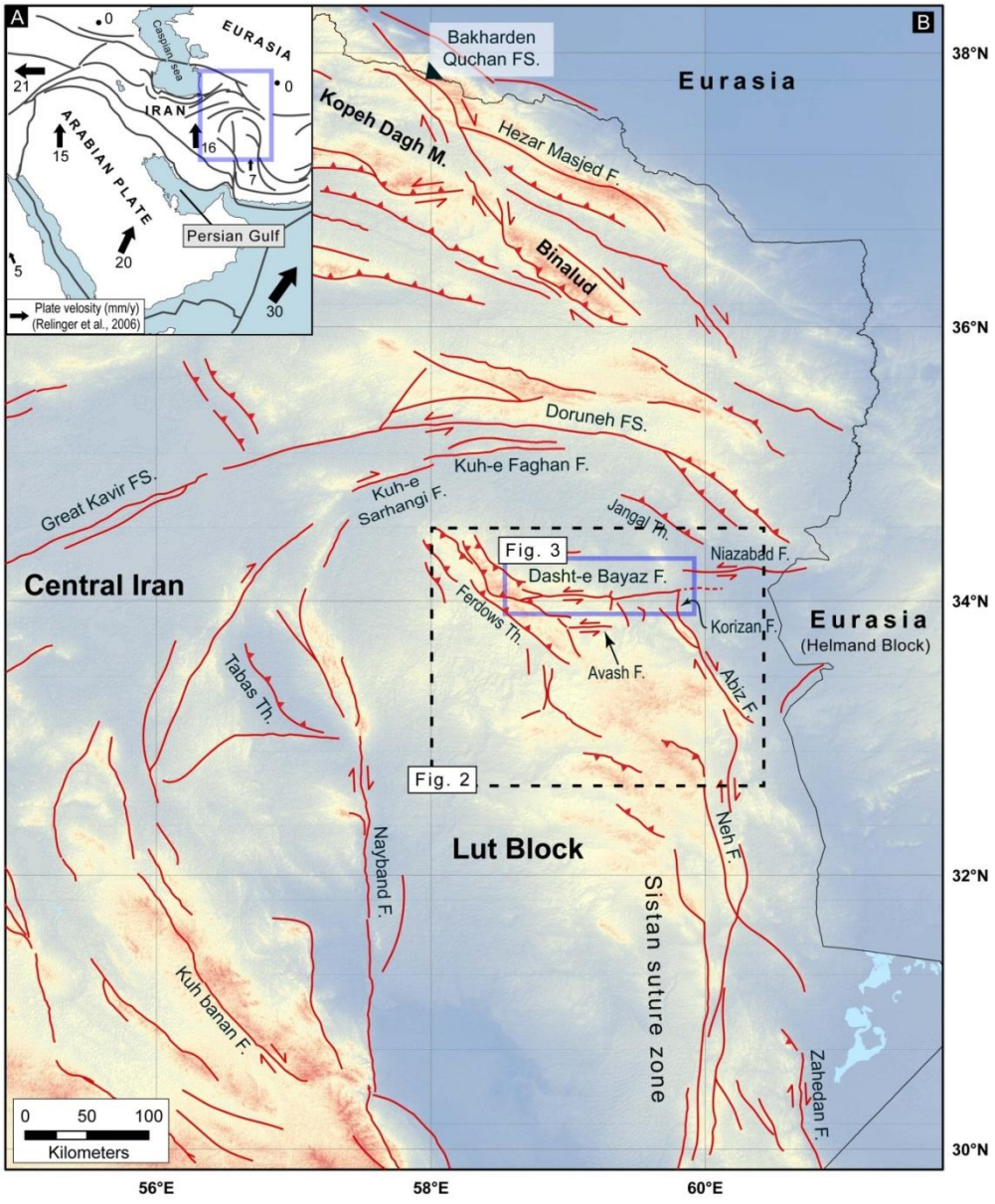

Figure 1. General tectonic map of the east and northeastern Iran. (A) The location of the study area (blue rectangle) in the Arabia–Eurasia collision framework (after Shabanian et al., 2010). Grey arrows and associated numbers represent Arabia–Eurasia plate velocities (mm/yr) after Reilinger et al. (2006). Solid lines are boundaries of plates or major blocks. (B) GTOPO30 topographic image showing the regional tectonic setting and the major active faults (red lines) in E and NE Iran. The study area of Dasht-e Bayaz is marked by the black dashed rectangle. Reverse/thrust faults are marked by small triangles pointing to the fault hanging wall. The fault map is based on Hessami et al. (2003), Walker and Jackson (2004), Shabanian et al. (2010), Farbod et al. (2011), Nozaem et al. (2013), Calzolari et al. (2015) and this study.

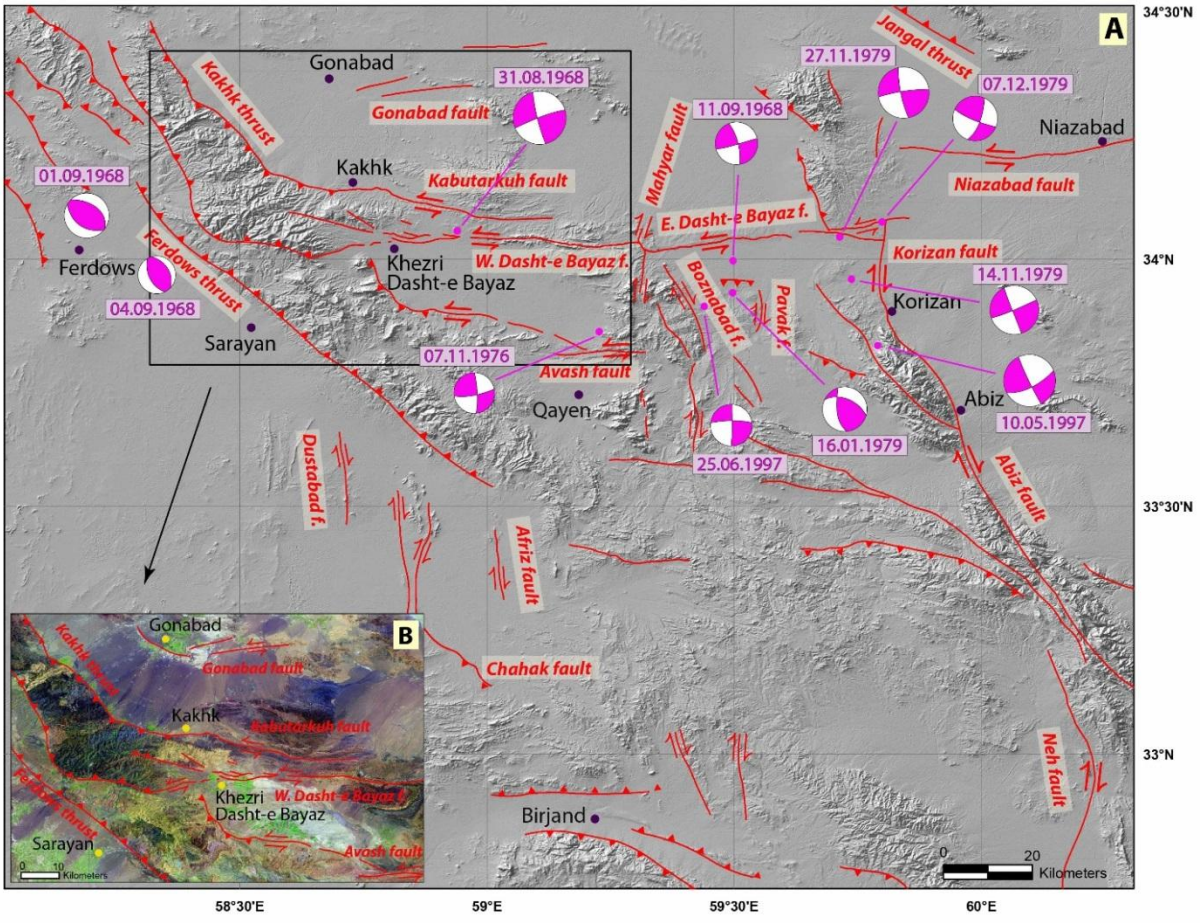

Figure 2. Map of the major active faults around the Dasht-e Bayaz area. (A) Major fault zones and their structural interactions in the area of interest. Focal mechanism solutions belong to the major earthquakes of the study area (redrafted from waveform modeling of Walker et al., 2004 and 2011). (B) LANDSAT ETM satellite overview (RGB, 541) of the area emphasizing the western termination of the left-lateral Dasht-e Bayaz, Kabutarkuh and Avash faults.

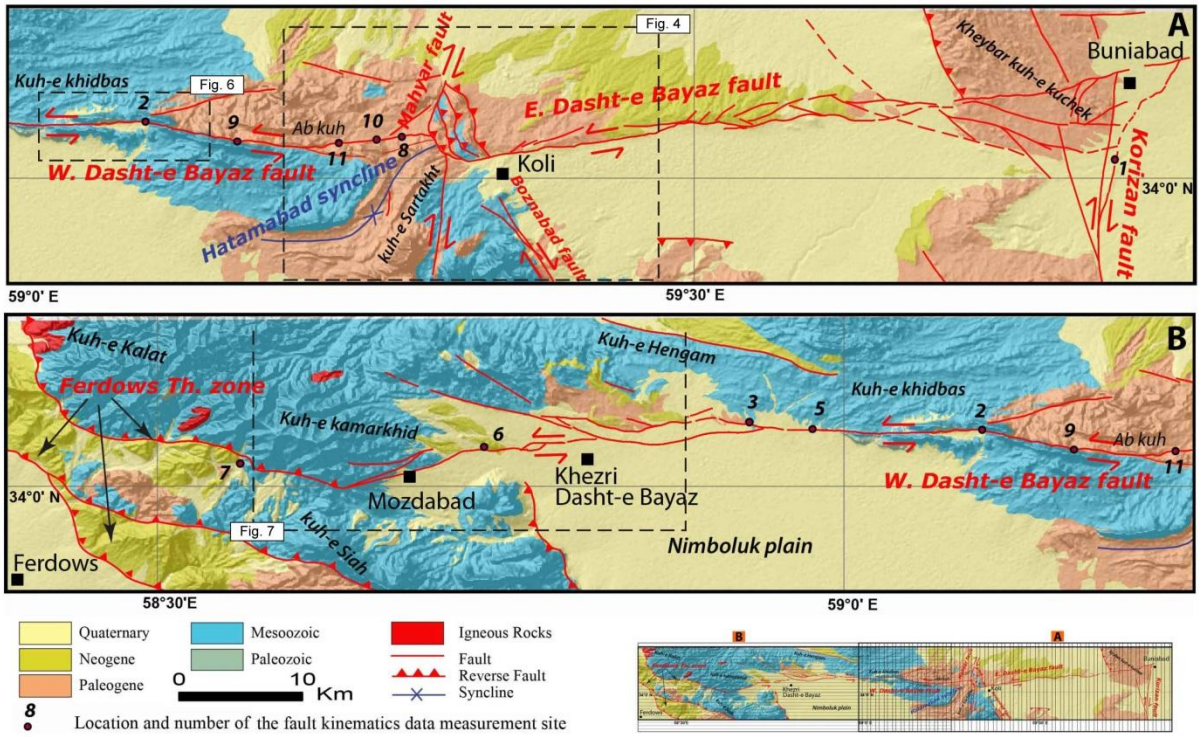

Figure 3. Simplified geological map of the Dasht-e Bayaz area based on published geological maps of the area (Alavi Naini and Behruzi, 1983; Fauvelet and Eftekhar Nezhad, 1991). Fault traces were extracted from satellite images complemented by field observations; we used Tchalenko and Berberian (1975) maps for the co-seismic ruptures in the northern Nimboluk plain, which currently is under cultivation.

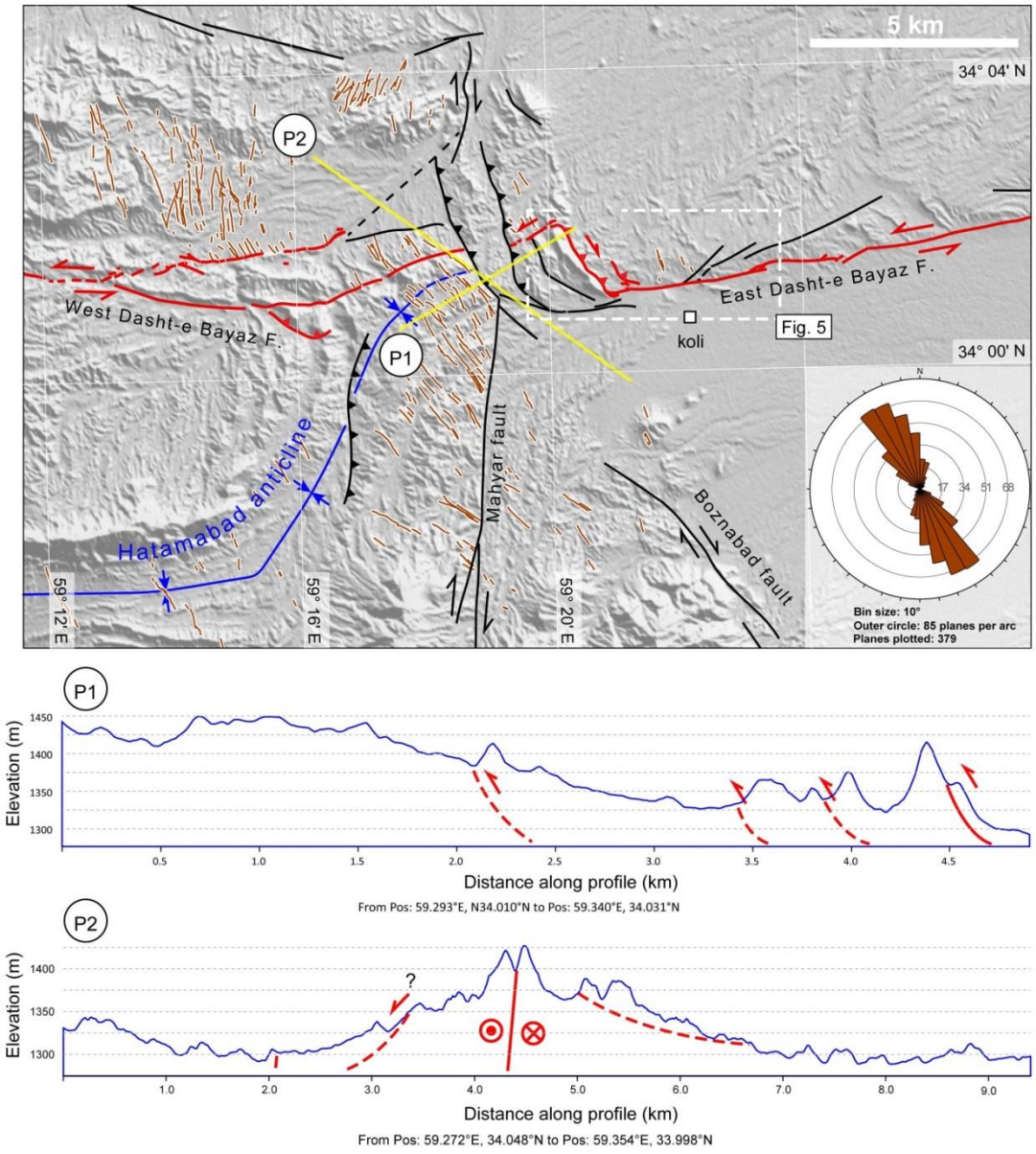

Figure 4. Morpho-structural map of the central intersection zone along the Dasht-e Bayaz fault. (A) Detailed fault map of the interaction zone of the Mahyar and the Dasht-e Bayaz faults. Solid black line is geological fault; inferred fault is shown by dashed black line. Red solid line is the coseismic rupture of the Dasht-e Bayaz 1968 (west of the Mahyar fault) and 1979 (east of the Mahyar fault) earthquakes. The N-S dextral and E-W sinistral fault zones displaced each other in the sense of their movement of about 1.5 km; see Figure 17 for more details on the structural configuration of this zone. The lower right rose diagram (rosette) indicates the frequency of orientations of post-folding dikes (cut by strike-slip faults) concentrated around the intersection zone; note that the overall orientation of N330±10°E does not significantly vary along the strike-slip faults. Two topographic profiles across the contractional (P1) and extensional (P2) quadrants are shown.

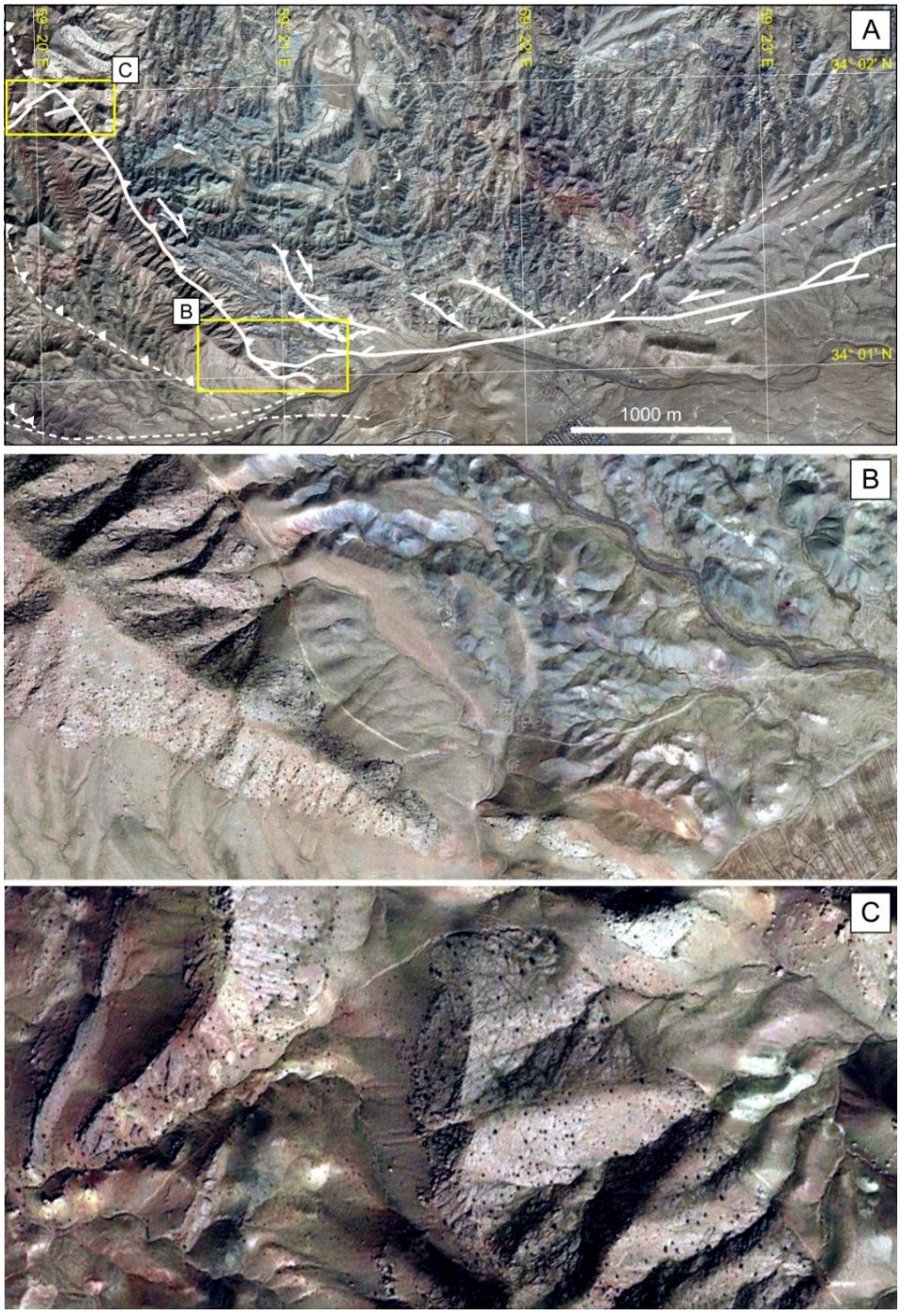

Figure 5. Bing Map image (SAS.Planet© 2015-2017) centered on the western termination of the East Dasht-e Bayaz fault. See Figure 3 for location. (A) Detailed fault map of the area. Solid white lines are coseismic rupture traces and dashed white lines are geological faults not reactivated during the 1979 Dasht-e Bayaz earthquake. (B) Close-up view of the sinistral rupture that terminates in a NE-dipping reverse segment. (C) Close-up view of the northern end of the reverse fault segment due to intersection with a SW-trending sinistral segment.

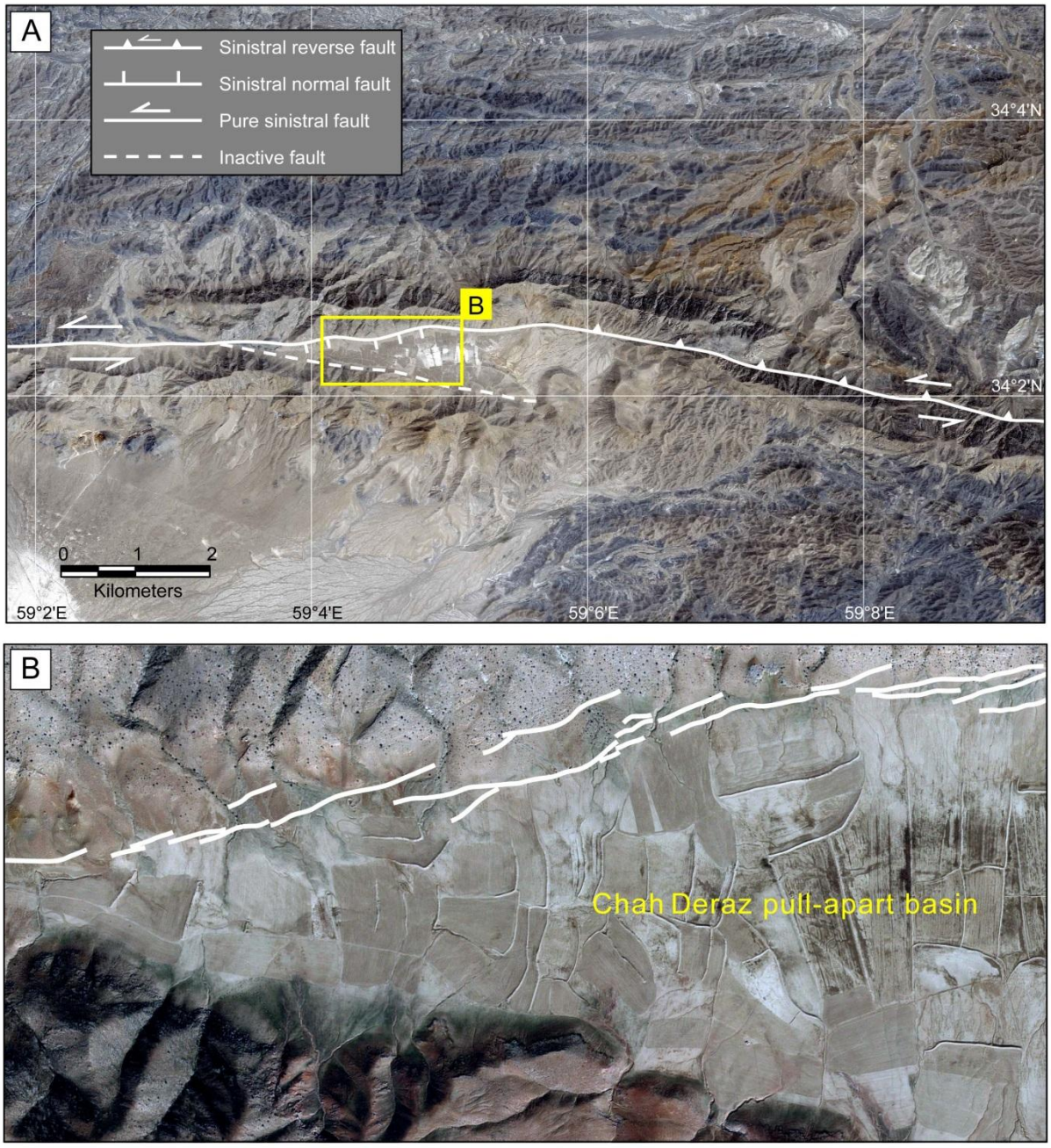

1144

1145 **Figure 6.** SPOT image of the Chah Deraz pull-apart basin along the west Dasht-e Bayaz fault. (A)
1146 the active trace of the fault passes at the northern margin of the basin, while the southern one is inactive.
1147 (B) close-up view of the coseismic rupture (1968 Dasht-e Bayaz earthquke) at the northen margin of the
1148 basin.

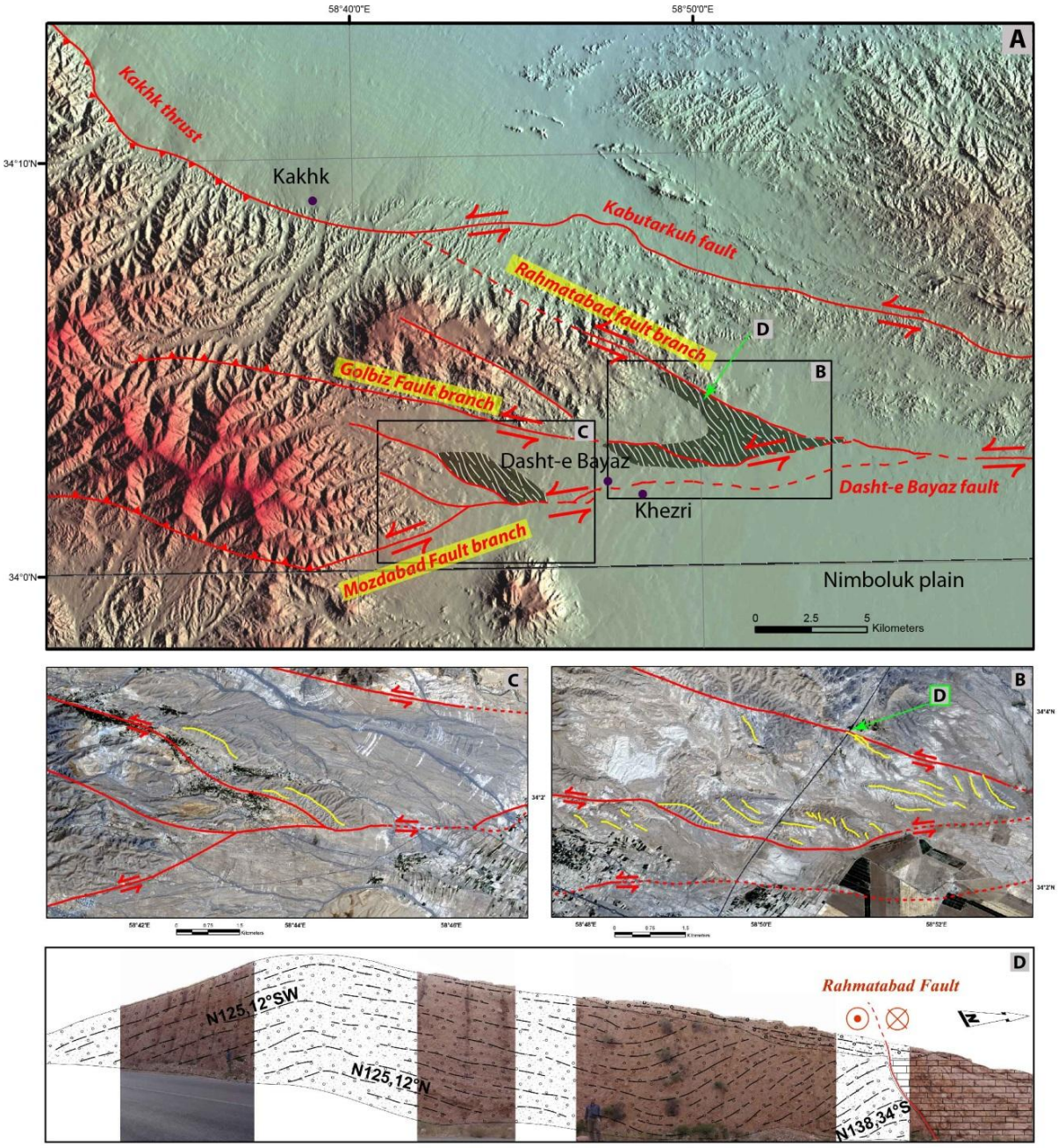

1149

1150 **Figure 7.** Tectonic features of the western portion of the west Dasht-e Bayz fault. (A) Shaded relief
1151 image of the northern Nimboluk plain and structural map of this area including different fault branches of
1152 the Dasht-e Bayaz fault. The hatched polygon shows areas involved in en-echelon folding and pressure
1153 ridges. (B) and (C) SPOT image of the Northern Nimboluk plain. Fold axes shown as yellow lines. (D)
1154 West looking photographs and reconstructed section across the Rahmatabad fault branch and associated
1155 folding of Plio-Quaternary deposits in the footwall.

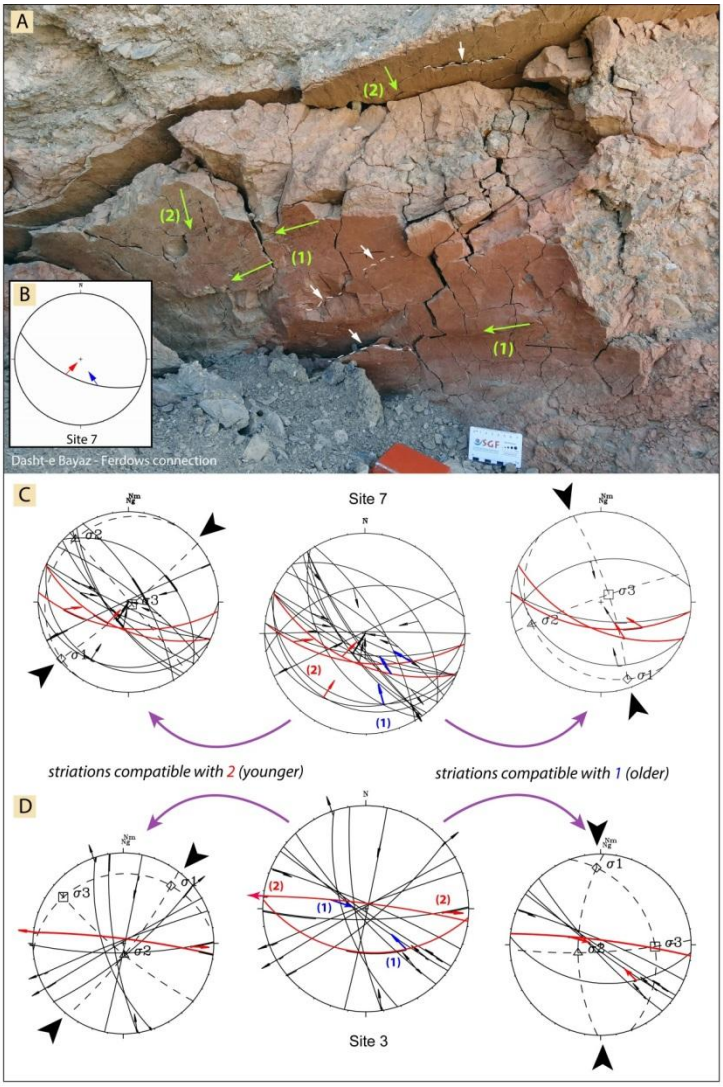

Figure 8. Distinct fault slips related to the modern and intermediate states of stress and a summary of data separation strategy applied in this study. (A) SE looking field photograph a fault plane (site 7) that includes two generations of striations and (B) a stereoplot of these striations. (1) and (2) refer to older and younger relative chronologies, respectively, of the striations on the fault plane in the Neogene mudstone. This site is along the western end of the Dasht-e Bayaz fault where it merges the Ferdows reverse fault zone. (C) The schmidt lower hemisphere stereographic projection of the fault slip data measured in site 7. (D) The lower hemisphere stereographic projection of the fault slip data measured in site 3. The middle diagram is non-separated data set including all fault slip data. (1) and (2) refer to the older and younger relative chronology of the striations. The stereograms (1) and (2) indicate relative chronology of two distinct sets of data. The relative chronology of striations is according to cross-cutting relationships observed on fault planes (colored as red). This strategy is applied to other sites for separation of fault slip data into homogenous data sets.

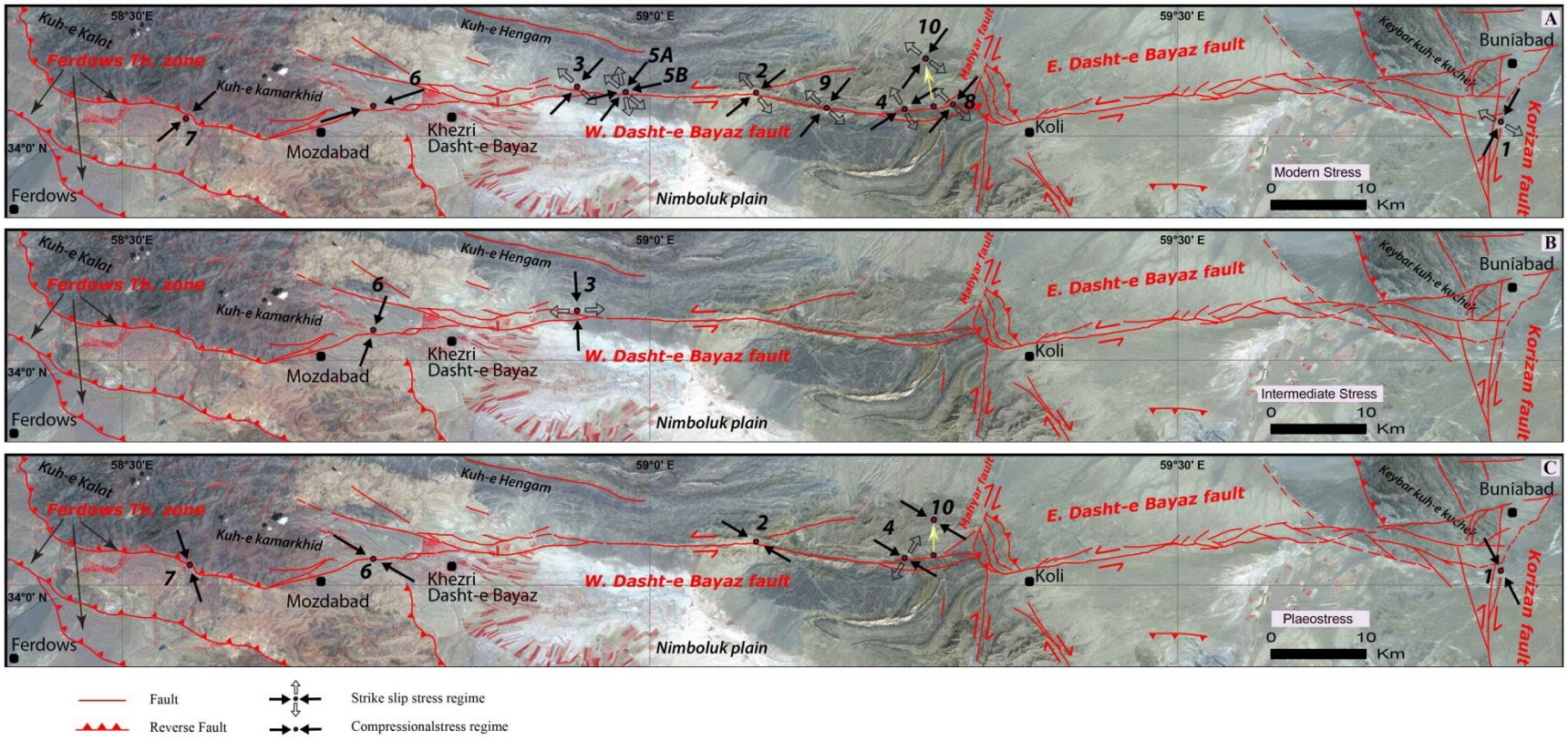

Figure 9. Reconstruction of the Plio-Quaternary stress fields in the Dasht-e Bayaz area, the base is ASTER image (RGB, 321). Direction of Maximum horizontal stress axis (σ1) for different stress fields showing dominant stress regimes including strike-slip, compressional and extensional deducted from inversions of fault kinematics data in each sites (see Table 2). (A) Modern state of stress (B) Intermediate state of stress (C) Paleostress state of stress.

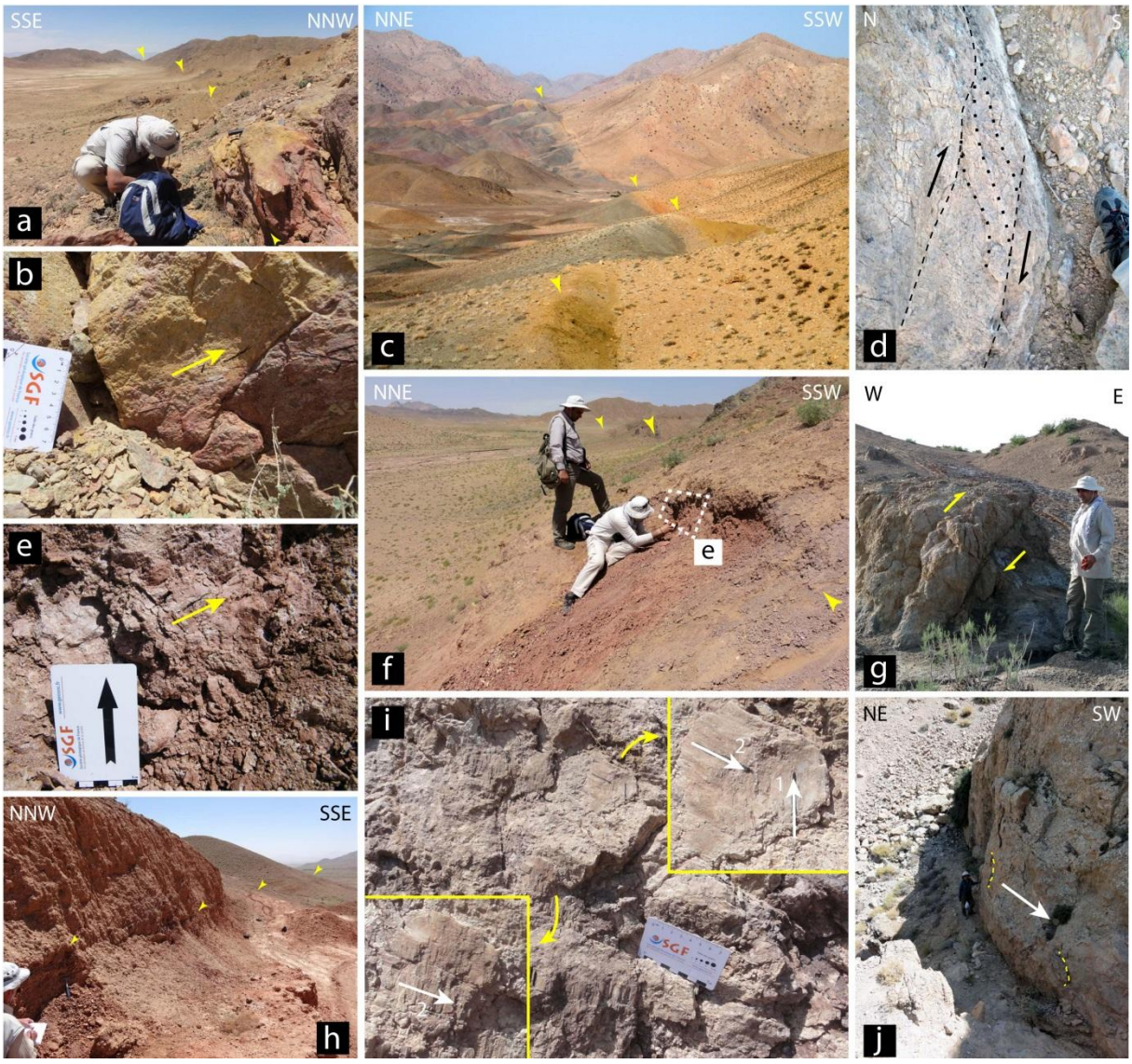

Figure 10. Field photographs of some of sites we have inspected for the measurement of fault slip data along the Dasht-e Bayaz fault. (a) Site 2 at the northern margin of the Chah Deraz pull-apart basin. (b) A northwards view of the fault plane and the associated sinistral striation in site 2. (c) general view of the Dashte- Bayaz earthquake rupture to the west of the intersection zone. (d) structural evidence of an ancient dextral faulting along the main trace of the Dasht-e Bayaz fault in the Chah Deraz pull-apart basin. (e) and (f) fault plane and striation of the fault measured along the coseismic rupture. (g) An outcrop of the northern continuation of the Korizan fault in site 1. (h) The reverse-sinistral fault trace in Neogene deposits in site 6. (i) a fault plane with two distinct generation of striations in site 10. (j) a metric scale sinistral fault plane along the main fault zone in site 9.

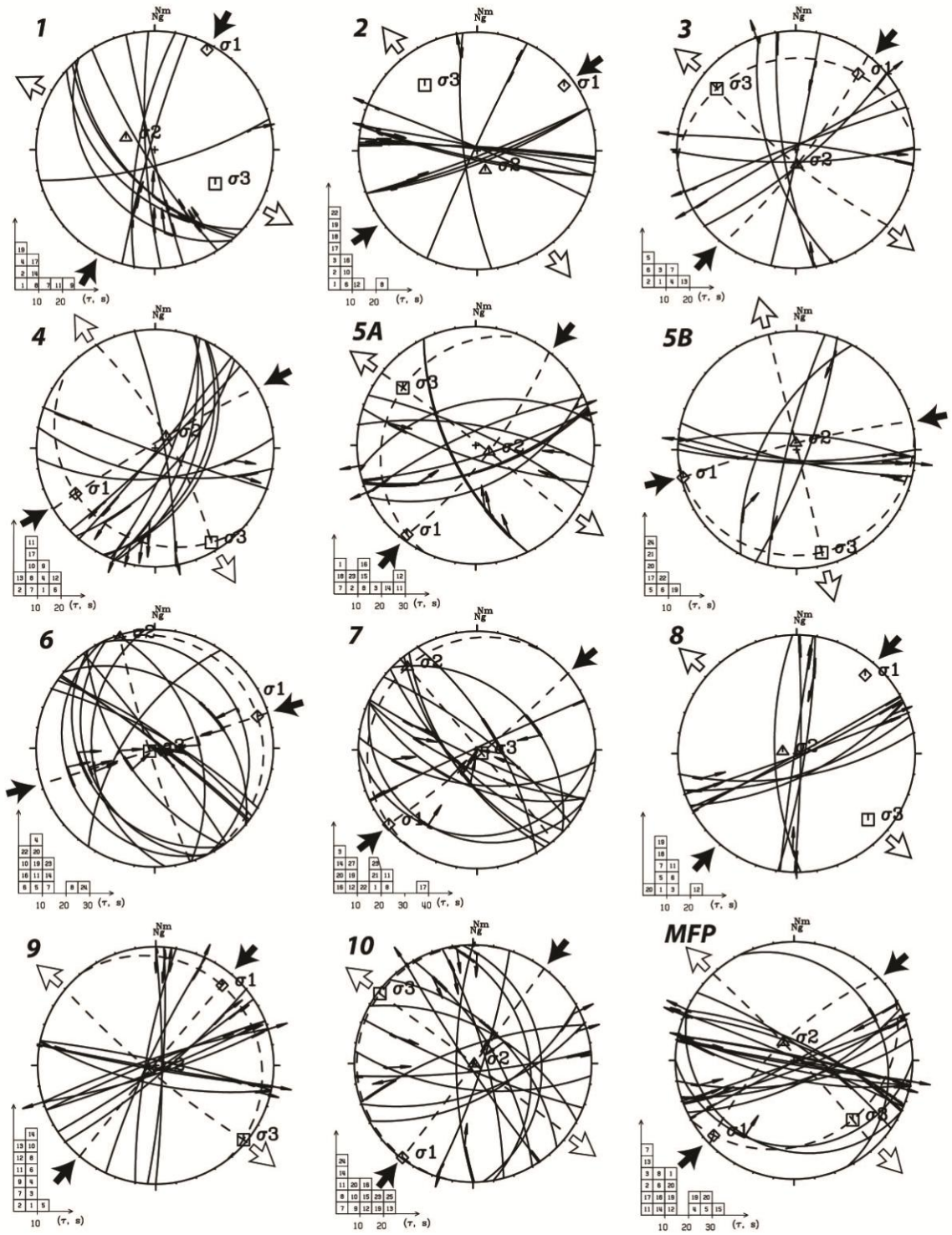

Figure 11. Lower hemisphere stereograms of fault slip data with inversion results of the modern state of stress presented in Table 1. Fault planes and measured slip vectors (arrows on fault planes) are plotted. Large arrows outside stereograms represent the direction of minimum (σ_3, divergent, white arrows) and maximum (σ_1) horizontal stress axes. Histograms show distribution of deviation angles between the measured and calculated slip vectors (e.g., *Bellier and Zoback*, 1995). Numbers on top left of stereograms refer to site marked in Figure 9 as well as in Table 1. MFP refers to result of inversion of major fault plane data.

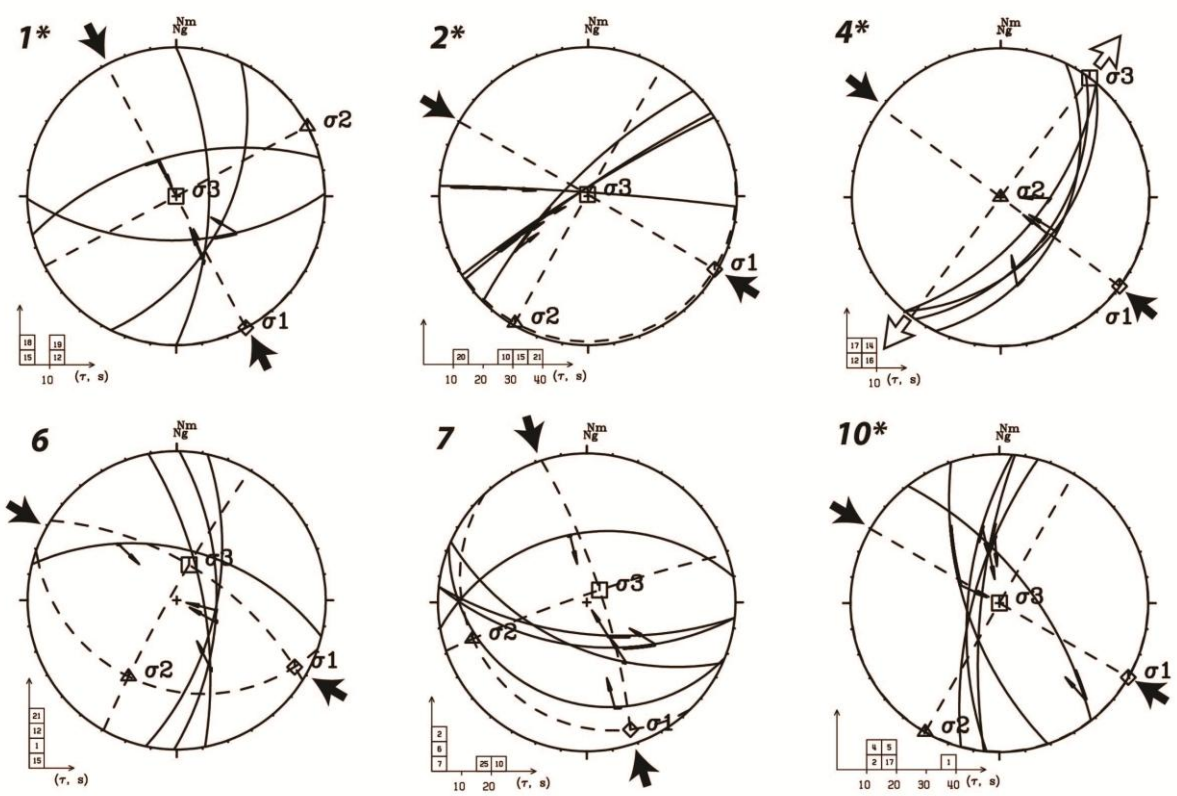

Figure 12. Lower hemisphere stereograms of fault slip data with inversion results of the paleostress state presented in Table 1. Numbers on top left of stereograms refer to site marked in Figure 9 as well as in Table 1. The stereograms indicated by asterisk are the "fixed" solutions (Bellier and Zoback, 1995) for fault data populations comprised of less than four well-distributed fault directions. See the caption of Figure 11 for stereoplot descriptions.

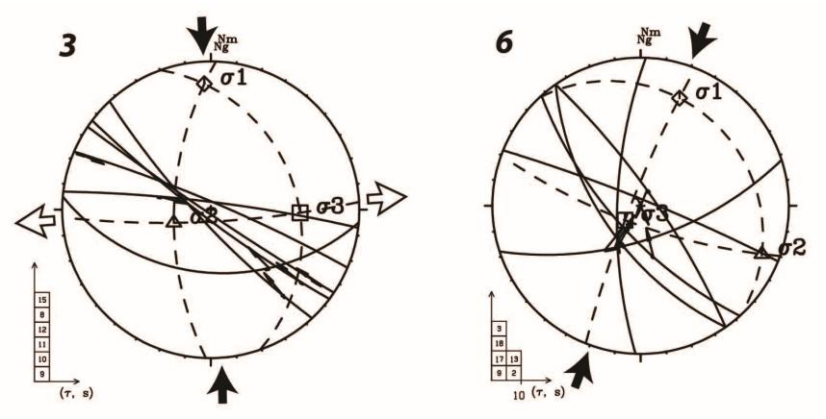

Figure 13. Lower hemisphere stereograms of fault slip data with inversion results of the intermediate state of stress presented in Table 1. Numbers on top left of stereograms refer to site marked in Figure 9 as well as in Table 1. See the caption of Figure 11 for stereoplot descriptions.

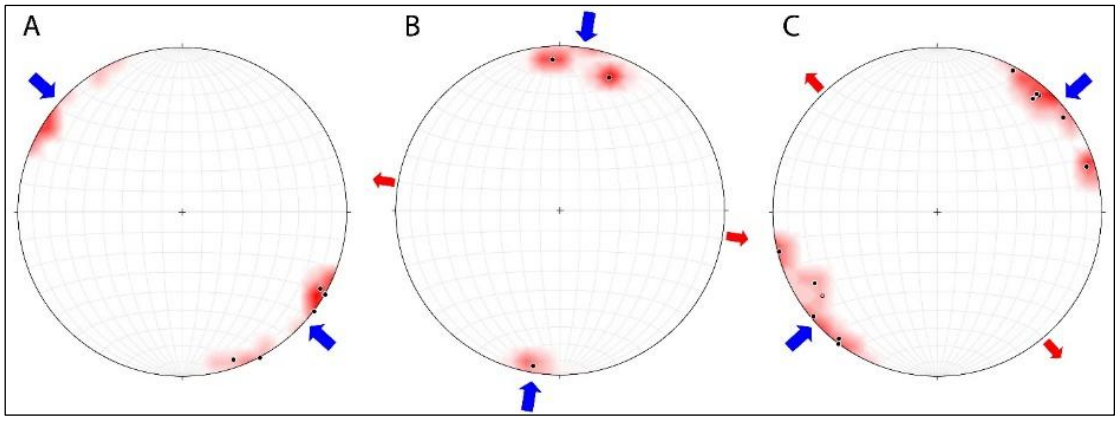

Figure 14. Lower hemisphere stereograms showing statistical analysis of the preferred direction of the maximum horizontal stress axis (σ_1) corresponding to (A) paleostress state (N135 ±15°E), (B) intermediate state of stress (N009±10°E) and (C) modern state of stress (N45±05°E); all calculated in PBT axes method (Marrett and Allmendinger, 1990; Allmendinger et al., 2013). Blue and red arrows indicate the mean direction of σ_1 and σ_3, respectively.

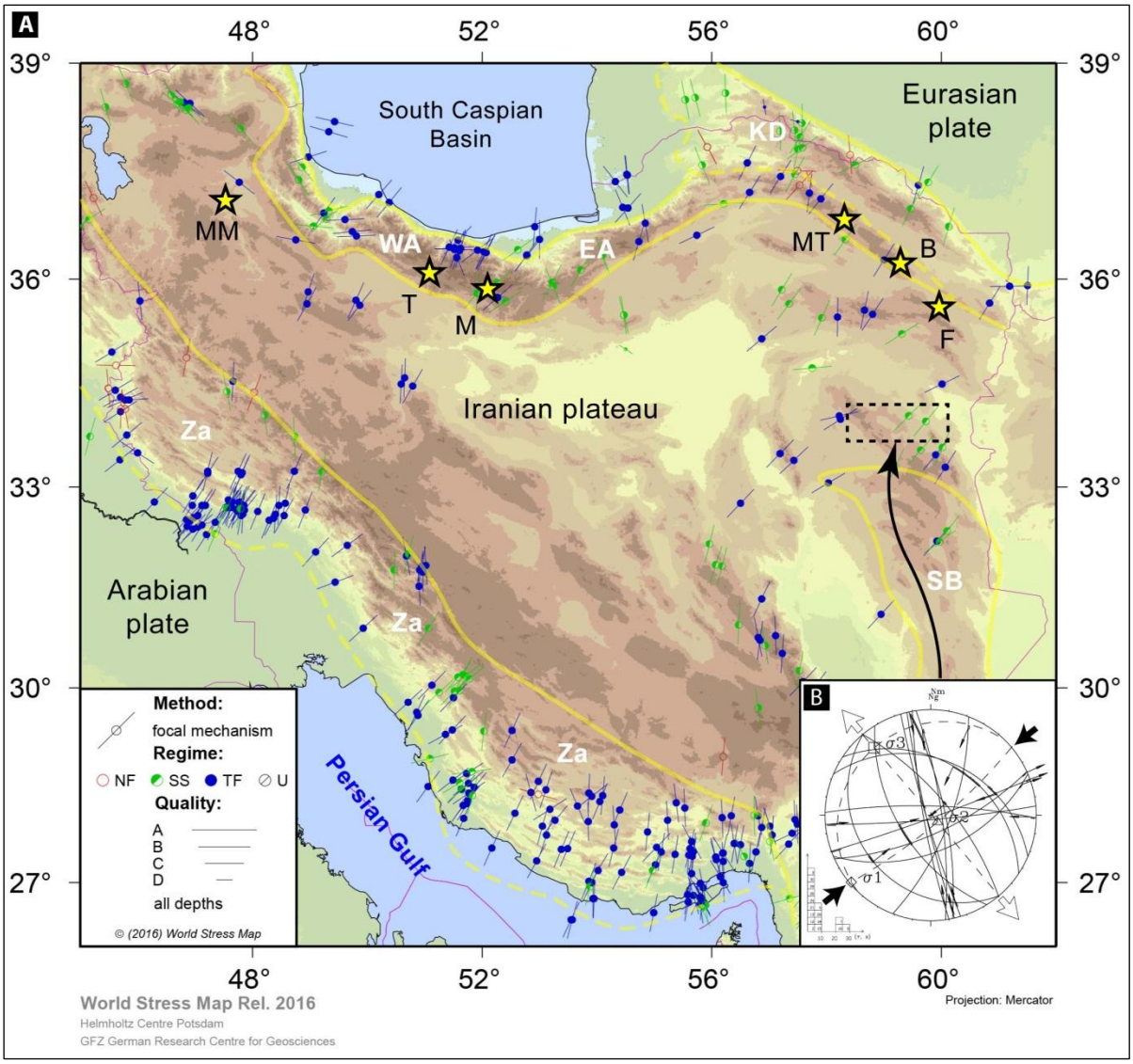

Figure 15. Stress map of the Iranian plateau and surrounding mountain belts. (A) $S_H$max orientations deriving from some of earthquake focal mechanisms in the Iranian plateau created by online stress map creator: http://www.world-stress-map.org/casmo/ (see Heidbach et al., 2016 and references therein). Abbreviation is: TF, thrust faulting; SS, strike-slip; NF, normal faulting; U, unknown; B, Binalud; KD, Kopeh Dagh; EA, eastern Alborz; WA, western Alborz; MT, Meshkan transition zone; F, Fariman town; SB, Sistan belt; Za, Zagros; M, Mosha; T, Taleghan; MM, Mahneshan - Mianeh . Different tectonic regimes are characterized by different symbol colors. NF and NS data is printed in red, SS data in green, and TF and TS data in blue. Data with an unknown regime is printed in black. (B) Our inversion results (N050±05°E trending σ_1) showing the present-day state of stress in Dasht-e Bayaz area, source parameters were used from instrumentally recorded earthquakes that have been modeled using body waves (Walker et al., 2004), see the caption of Table 2 for more details. We put into practice inversion of focal mechanisms by using moderate to large earthquakes (7.1>M>5.7) and employing the method proposed by Carey-Gailhardis and Mercier (1987).

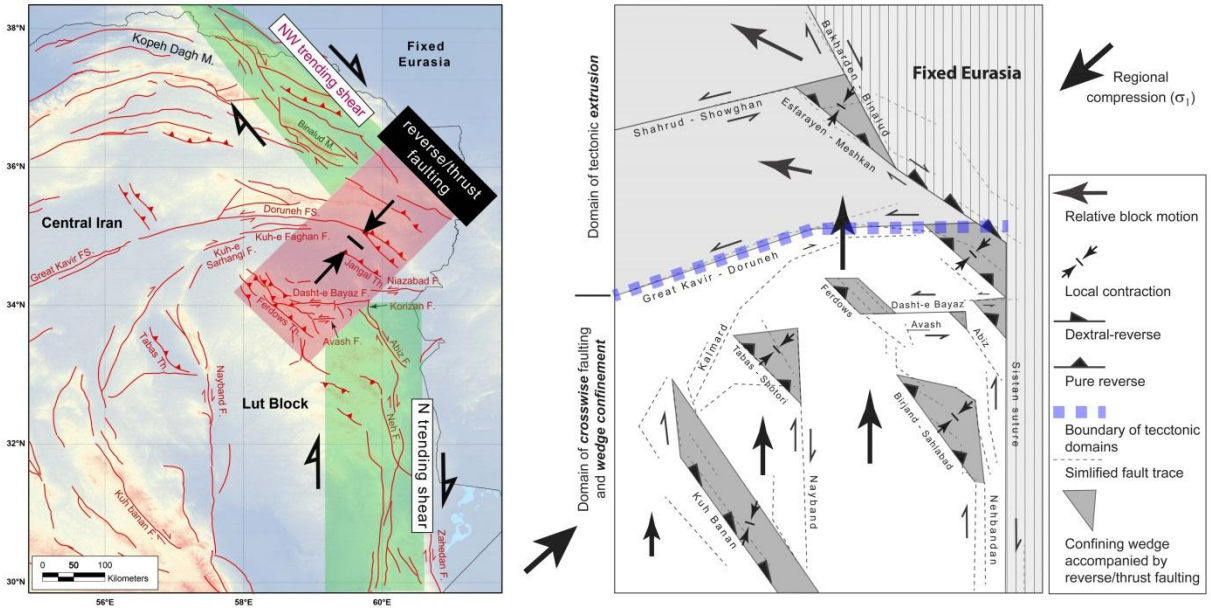

Figure 16. A brief explanation of our model about the northern Lut block and the southern Kopeh Dagh domain. (A) Up to latitude 34° N the majority of convergence is accommodated by right-lateral shear between Iranian plateau and fixed Eurasia. To the north of latitude 34° N, an interruption in right-lateral shear takes place and in the absence of right-lateral shear, convergence is accommodated by reverse/thrust faulting. (B) Schematic model emphasizing the role of separated thrust zones, as confining wedges at the termination of N-S dextral fault, in accommodation of the Arabia-Eurasia convergence. See text for more information.

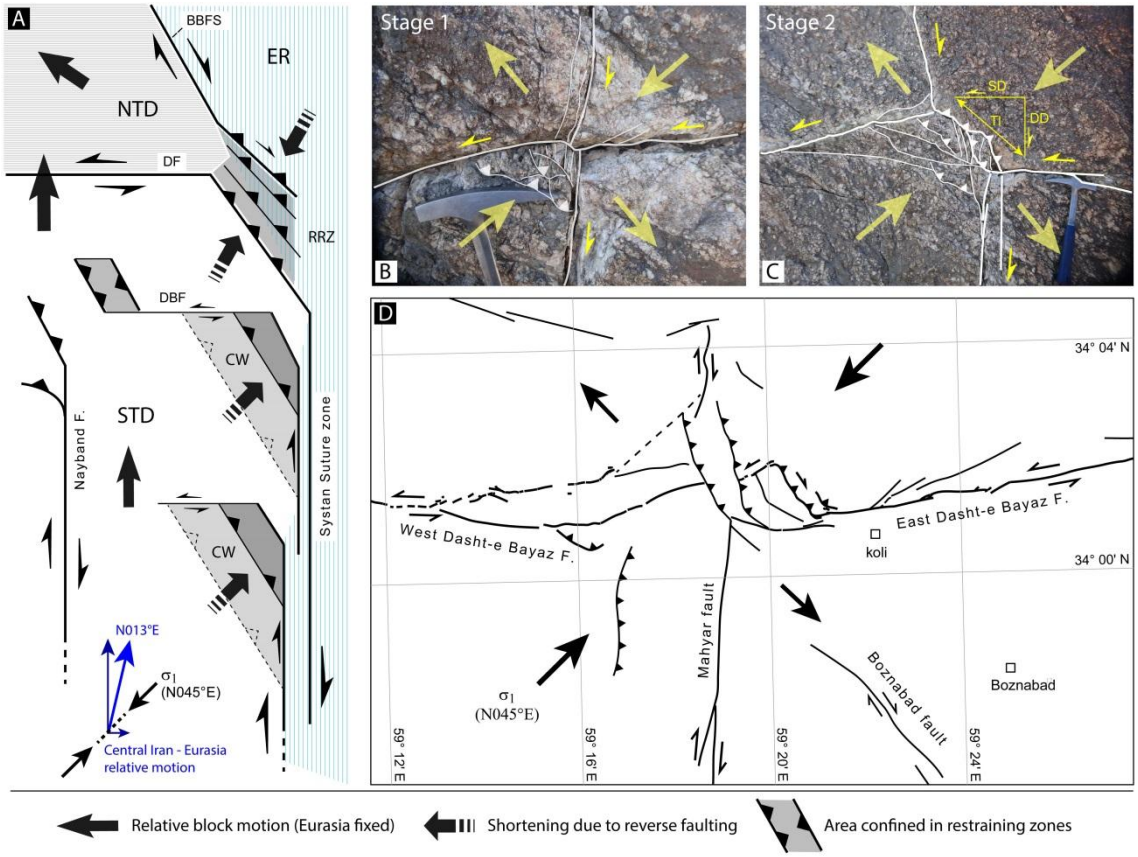

Figure 17. Details on the processes involved in the accommodation of Lut – Eurasia convergence in the NE and E Iranian regions. (A) The process of wedge confining at the edges of north-going blocks and the associated secondary sinistral faulting along E-W faults such as the Dasht-e Bayaz and Niazabad. The overall N013°E direction of Lut – Eurasia motion (Walpersdorf et al., 2014) is mainly taken up by lithospheric N-S dextral shear translating the southern tectonic domain (STD) northwards. Shortening at the opposing edges of the main blocks (STD against ER) is accommodated through reverse faulting in a restraining relay zone (RRZ in "A"; Farbod, 2012; Aflaki et al., 2019), while internal deformations due to sub-block adjustments is taken up by crosswise dextral and sinistral faulting accompanied by contractional deformation at their terminations (CW, confining wedge); BBFS, Bakharden – Binalud fault system; DF, Doruneh fault; DBF, Dasht-e Bayaz fault. (B) And (C) Site-scale examples for the evolution of crosswise faulting; (B) illustrates the initial stage of crosswise faulting and (C) shows the structural configuration of crosswise dextral and sinistral faults after development of contractional quadrants. "TL" is the length of the main thrust fault zone developed perpendicular to the compression and is proportional to the amount of dextral (DD) and sinistral (SD) displacements of the main crosswise fault traces. (D) The intersection zone between the Dasht-e Bayaz and Mahyar faults; note to the analogy between this structural configuration and the typical crosswise faulting illustrated in (C). Such kind of kinematic interaction accommodates the overall convergence oblique to the faults without a need for rotations of faults and blocks around vertical axes.

Table 1

The fault kinematic inversion results characterizing the Pliocene-Quaternary stress regimes in the Dasht-e Bayaz area.

Site	Long.	Lat.	Paleostress							Modern Stress							Intermediate Stress							Lithology	Age
	(°E)	(°N)	Stress axis(trend/plunge)			R	N	Q	Rm	Stress axis(trend/plunge)			R	N	Q	Rm	Stress axis(trend/plunge)			R	N	Q	Rm		
			σ1	σ2	σ3					σ1	σ2	σ3					σ1	σ2	σ3						
1	59.807	34.013	152/00	62/00	295/90	0.595	4	CF	C	28/03	293/61	119/29	0.51	10	B	S	-	-	-	-	-	-	-	Andesite	Paleo-Eocene
2	59.101	34.041	120/01	210/01	345/89	0.500	4	CF	C	53/05	157/70	321/19	0.47	12	A	S	-	-	-	-	-	-	-	Sandstone	Triassic
3	58.931	34.048	-	-	-	-	-	-	-	40/11	176/75	308/10	0.55	8	A	S	357/9	250/60	92/28	0.44	6	C	S	Conglomerate	Quaternary
4	59.248	34.026	127/00	303/90	37/00	0.327	4	CF	S	240/15	43/75	149/04	0.43	12	A	S	-	-	-	-	-	-	-	Andesite	Paleo-Eocene
5A	58.977	34.043	-	-	-	-	-	-	-	218/03	116/76	308/14	0.66	12	A	S	-	-	-	-	-	-	-	Conglomerate	Quaternary
5B	58.977	34.043	-	-	-	-	-	-	-	256/01	354/83	166/07	0.714	8	A	S	-	-	-	-	-	-	-	Conglomerate	Quaternary
6	58.738	34.028	119/05	212/28	19/62	0.452	4	C	C	73/06	343/01	241/84	0.23	14	B	C	20/15	112/07	227/74	0.12	6	A	C	Conglomerate	Pliocene
7	58.561	34.017	161/06	252/12	46/76	0.696	5	B	C	230/02	320/05	124/85	0.78	14	A	C	-	-	-	-	-	-	-	Conglomerate	Pliocene
8	59.281	34.032	-	-	-	-	-	-	-	41/07	279/76	133/11	0.96	10	A	S	-	-	-	-	-	-	-	Tuff	Paleocene
9	59.168	34.027	-	-	-	-	-	-	-	40/07	232/82	130/2	0.530	14	A	S	-	-	-	-	-	-	-	Dolomite	Triassic
10	59.274	34.028	120/00	210/00	354/90	0.6	5	CF	C	217/00	103/89	307/01	0.624	15	A	S	-	-	-	-	-	-	-	Limestone	Paleocene

Note: Site numbers and their geographic coordination refer to Figure 9. The results of inversion of fault slip data are including trend and plunge of principal stress axes (σ1, σ2, σ3 (matching maximum, intermediate and minimum stress axes, respectively) and stress ratio "R= (σ2-σ1) / (σ3-σ1)" shows the relative stress magnitude. N, number of fault slip data involved in stress calculations; Rm points out to stress regimes: C, compressional; S, strike-slip; Q indicates the quality of stress tensors: A, well-constrained; B, constrained; C, poorly-constrained solutions. CF quality represents data sets consist of less than four spatially well-distributed fault slip data, for this kind of data sets a "fixed" solutions (Bellier and Zoback, 1995) is used, in which the principal stress axes were fixed to lie in horizontal and vertical planes. In site 5, two deviatoric stress tensors (5A and 5B) were obtained.

Table 2

Earthquake source parameters used in the focal mechanism inversion.

Date	Time (UTC)	Y	X	Depth (km)	Magnitude (Mw)	Strike	Dip	Rake	Reference
1968.08.31	10:47	34.068	59.018	17	7.1m	254	84	5	5
1968.08.31	10:47	34.068	59.018	10	6.4	320	70	90	5
1968.09.01	07:27	34.099	58.155	9	6.3	115	54	85	3
1968.09.04	23:24	34.042	58.244	9	5.5	148	56	81	3
1968.09.11	19:17	34.031	59.472	6	5.6	78	90	16	1
1976.11.07	04:00	33.836	59.171	8	6.0m	84	79	12	1,4
1976.11.07	04:00	33.836	59.171	10		67	52	-7	1
1979.01.16	09:50	33.961	59.501	11	6.5m	293	34	46	1,4
1979.01.16	09:50	33.961	59.501	13		257	88	5	1
1979.11.14	02:21	34.017	59.78	10	6.6m	160	89	-177	1,4
1979.11.14	02:21	34.017	59.78	6		85	85	1	1
1979.11.27	17:10	34.056	59.769	8	7.1m	261	82	8	5
1979.12.07	09:24	34.13	59.889	10	5.9	113	84	21	1
1997.05.10	07:57	33.88	59.815	13	7.2	156	89	-160	2
1997.06.25	19:38	33.972	59.459	8	5.7	181	87	170	2

Note: In this research we used the source parameters of instrumentally recorded earthquakes in the Dasht-e Bayaz region that have been modeled by Walker et al. (2004) with body wave methods. References are the same as they used in their modeling, including: (1) Baker (1993), (2) Berberian et al. (1999), (3) Walker et al. (2003), (4) Jackson (2001) and (5) Walker et al. (2004). An (m) after of some of Mw means a multiple event. For more information see Table 1 of Walker et al. (2011).

Table 1

Click here to download Table: Table 1.docx

Table 1

The fault kinematic inversion results characterizing the Pliocene-Quaternary stress regimes in the Dasht-e Bayaz area.

Site	Long.	Lat.	Paleostress							Modern Stress							Intermediate Stress							Lithology	Age
	(°E)	(°N)	Stress axis(trend/plunge)			R	N	Q	Rm	Stress axis(trend/plunge)			R	N	Q	Rm	Stress axis(trend/plunge)			R	N	Q	Rm		
			σ1	σ2	σ3					σ1	σ2	σ3					σ1	σ2	σ3						
1	59.807	34.013	152/00	62/00	295/90	0.595	4	CF	C	28/03	293/61	119/29	0.51	10	B	S	-	-	-	-	-	-	-	Andesite	Paleo-Eocene
2	59.101	34.041	120/01	210/01	345/89	0.500	4	CF	C	53/05	157/70	321/19	0.47	12	A	S	-	-	-	-	-	-	-	Sandstone	Triassic
3	58.931	34.048	-	-	-	-	-	-	-	40/11	176/75	308/10	0.55	8	A	S	357/9	250/60	92/28	0.44	6	C	S	Conglomerate	Quaternary
4	59.248	34.026	127/00	303/90	37/00	0.327	4	CF	S	240/15	43/75	149/04	0.43	12	A	S	-	-	-	-	-	-	-	Andesite	Paleo-Eocene
5A	58.977	34.043	-	-	-	-	-	-	-	218/03	116/76	308/14	0.66	12	A	S	-	-	-	-	-	-	-	Conglomerate	Quaternary
5B	58.977	34.043	-	-	-	-	-	-	-	256/01	354/83	166/07	0.714	8	A	S	-	-	-	-	-	-	-	Conglomerate	Quaternary
6	58.738	34.028	119/05	212/28	19/62	0.452	4	C	C	73/06	343/01	241/84	0.23	14	B	C	20/15	112/07	227/74	0.12	6	A	C	Conglomerate	Pliocene
7	58.561	34.017	161/06	252/12	46/76	0.696	5	B	C	230/02	320/05	124/85	0.78	14	A	C	-	-	-	-	-	-	-	Conglomerate	Pliocene
8	59.281	34.032	-	-	-	-	-	-	-	41/07	279/76	133/11	0.96	10	A	S	-	-	-	-	-	-	-	Tuff	Paleocene
9	59.168	34.027	-	-	-	-	-	-	-	40/07	232/82	130/2	0.530	14	A	S	-	-	-	-	-	-	-	Dolomite	Triassic
10	59.274	34.028	120/00	210/00	354/90	0.6	5	CF	C	217/00	103/89	307/01	0.624	15	A	S	-	-	-	-	-	-	-	Limestone	Paleocene

Note: Site numbers and their geographic coordination refer to Figure 9. The results of inversion of fault slip data are including trend and plunge of principal stress axes (σ1, σ2, σ3 (matching maximum, intermediate and minimum stress axes, respectively) and stress ratio "R= (σ2-σ1) / (σ3-σ1)" shows the relative stress magnitude. N, number of fault slip data involved in stress calculations; Rm points out to stress regimes: C, compressional; S, strike-slip; Q indicates the quality of stress tensors: A, well-constrained; B, constrained; C, poorly-constrained solutions. CF quality represents data sets consist of less than four spatially well-distributed fault slip data, for this kind of data sets a "fixed" solutions (Bellier and Zoback, 1995) is used, in which the principal stress axes were fixed to lie in horizontal and vertical planes. In site 5, two deviatoric stress tensors (5A and 5B) were obtained.

Table 2

Click here to download Table: Table 2.docx

Table 2

Earthquake source parameters used in the focal mechanism inversion.

Date	Time (UTC)	Y	X	Depth (km)	Magnitude (Mw)	Strike	Dip	Rake	Reference
1968.08.31	10:47	34.068	59.018	17	7.1m	254	84	5	5
1968.08.31	10:47	34.068	59.018	10	6.4	320	70	90	5
1968.09.01	07:27	34.099	58.155	9	6.3	115	54	85	3
1968.09.04	23:24	34.042	58.244	9	5.5	148	56	81	3
1968.09.11	19:17	34.031	59.472	6	5.6	78	90	16	1
1976.11.07	04:00	33.836	59.171	8	6.0m	84	79	12	1,4
1976.11.07	04:00	33.836	59.171	10		67	52	-7	1
1979.01.16	09:50	33.961	59.501	11	6.5m	293	34	46	1,4
1979.01.16	09:50	33.961	59.501	13		257	88	5	1
1979.11.14	02:21	34.017	59.78	10	6.6m	160	89	-177	1,4
1979.11.14	02:21	34.017	59.78	6		85	85	1	1
1979.11.27	17:10	34.056	59.769	8	7.1m	261	82	8	5
1979.12.07	09:24	34.13	59.889	10	5.9	113	84	21	1
1997.05.10	07:57	33.88	59.815	13	7.2	156	89	-160	2
1997.06.25	19:38	33.972	59.459	8	5.7	181	87	170	2

Note: In this research we used the source parameters of instrumentally recorded earthquakes in the Dasht-e Bayaz region that have been modeled by Walker et al. (2004) with body wave methods. References are the same as they used in their modeling, including: (1) Baker (1993), (2) Berberian et al. (1999), (3) Walker et al. (2003), (4) Jackson (2001) and (5) Walker et al. (2004). An (m) after of some of Mw means a multiple event. For more information see Table 1 of Walker et al. (2011).